

CHAPTER 1: INTRODUCTION

1.1 General overview

Photo thermal methods have been developed over the last 30 years to measure the properties of thin films or different samples. The film thickness can be measured knowing the thermal diffusivity of the film and the substrate on which the film has been deposited. Alternatively the thermal diffusivity of a thin sample may be measured knowing the thickness of the sample. These techniques are sometimes referred to as using the principles of “thermal interferometry”. In general the concept of thermal decay having wavelike behaviour is not widely understood and indeed the concept of thermal interferometry is only valid when the thermal diffusion length is greater than or comparable to the dimension (thickness) of the sample being measured. In such cases where the system under consideration has length scales much shorter than the thermal diffusion length, then the damping is relatively less important and the theory of scalar waves may be accepted to describe the wave nature of thermal diffusion.

Thermal interferometry has been an interesting area of photo thermal research in the past due to its complexity and potential applications in the automotive and health industries. However unlike optical interferometry it has not yet been successfully applied in industry. A number of optical interferometers including the Michelson Interferometer and Young’s Interferometer have been developed and used for various applications, but no success has been achieved so far in developing a thermal interferometer.

There has been considerable achievement on optical interferometry in the past, suggesting development of a Thermal Interferometer to test thermal properties of different materials, which are sensitive to optical radiation. The concept of thermal wave interference (termed as thermal wave interferometry) originates from the measurement of thermal diffusivity or thickness of thin films using the photo-acoustic effect, which is described as follows:

- In a photo-acoustic cell, a film sample absorbs a modulated light beam and converts it into thermal energy, which propagates in the sample as a complex thermal wave which decays quickly due to its highly damped nature. But in thin samples these thermal waves can travel forward and backward striking the rear and front surfaces of the sample many times before significantly decaying.
- This leads to periodic temperature variations on the sample surface, heating and

cooling the air layer in immediate contact with the surface. This air layer expands and contracts periodically, resulting in the formation of acoustic waves in the cell, which are detected by a pressure sensitive microphone.

- By comparing the phase lag between the modulated light beam and acoustic signals, the thermal diffusivity of the film sample can be worked out provided the thickness of the sample is known or vice-versa.

In the experimental set up a light source (say tungsten halogen), a thin film sample (such as copper) in an enclosed cell and an audio signal detector is used as a photo acoustic spectrometer. When the chopped incident light through an optical chopper is incident on the sample, a heat flow takes place and thermal waves travel from the inner surface to the outer surface of the sample resulting in temperature variations at the boundary gas layers inside the sample cell. This thin gas layer works as a piston, creating a pressure variation that generates acoustic waves in the cell. These acoustic waves can be detected by a sensitive microphone. In this process as heat takes a little time to diffuse from the front surface to the rear surface of the sample, a phase lag is produced between the incident chopped light (i.e. modulated light beam) and the detected acoustic signals and this phase lag will depend on thermal diffusivity and the thickness of the sample. There is an additional acoustic phase lag (say ϕ_a) due to the finite distance between the sample and the microphone, which is usually ignored as the acoustic wavelength is much greater than this distance. By utilising the phase lag, measurement of thermal diffusivity is done in the photo-acoustic effect.

The phase lag between the incident radiation and the generated acoustic waves is termed as, 'thermal phase lag' (say ϕ_T) in photo-acoustic spectroscopy. To derive equations relating thermal phase lag to the thermal properties of a material, two different approaches are usually adopted:

The first involves deriving thermal diffusion equations considering different boundary conditions, which accounts for the relationship between the temperature variation and the thermal properties for the front surface technique, as established by the Rosencwaig-Gersho theory (RG theory) [2] and further expanded by Charpentier [7] for the rear surface technique.

In the second approach Bennett and Patty [5] formulated the thermal response as a superposition of thermal waves on the sample surface using interference theory and recast the R-G theory.

The first approach is applicable to all cases, where boundary conditions are defined mathematically; however in the second approach the mathematical expression is simple but appears to be applicable only to special cases. Since then, several researchers have discussed thermal-wave interference and diffraction, such as Mandelis [16, 17]. Thus the concept of thermal wave interference can be applied to illustrate the thermal response of samples in the Photo acoustic cells.

The technique has potential commercial applications. For example, there have been earlier attempts by some researchers to use the photo acoustic technique to measure thickness and thermal properties of thermal barrier coatings using the variation in the reflection coefficients [25]. Also there is further scope for development of a commercial instrument for use in the health industry for the detection of protein, biomass etc. A deposited biomass or protein on back of a metal surface will change the reflection coefficient for thermal waves, which will result in an extra phase lag in the acoustic signals to be recorded. Thus using these parameters the thickness of deposition can be worked out. This example has been shown in the diagram below.

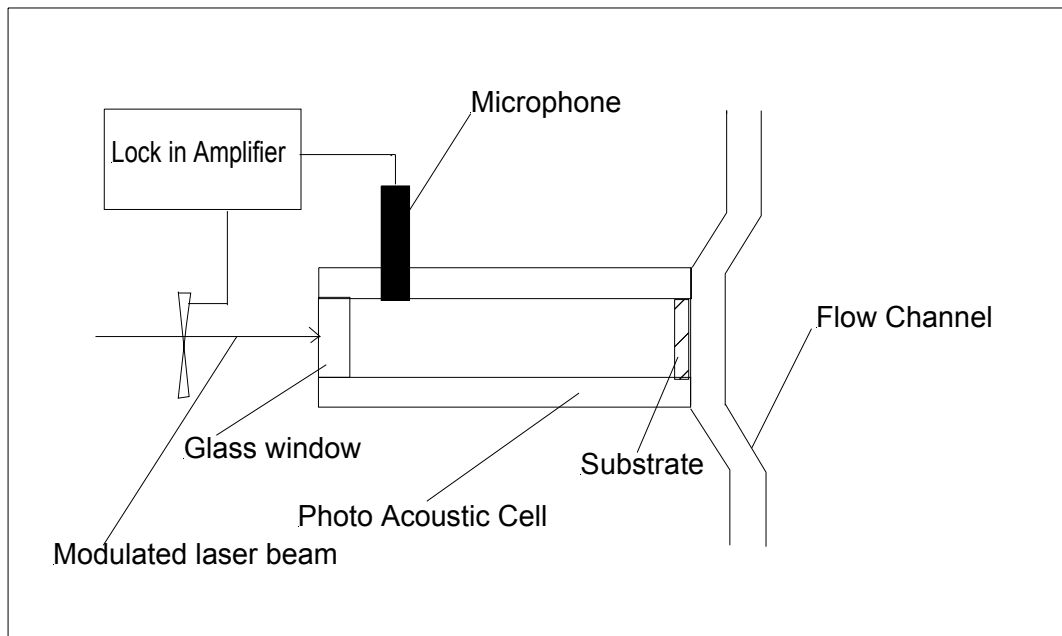


Figure 1.1 Schematic diagram of a device showing detection of biomass attachment

Due to the interface contacting the biomass, the thermal effusivity of the substrate would change and it has been theoretically proved and experimentally established [5, 24, and 25] in the measurements of thermal diffusivity for thin films. This device transforms the temperature variation into a measurable acoustic signal, which is detected and recorded by a microphone and lock-in amplifier. The additional phase lag of the acoustic signal with respect to the modulated light accounts for the thickness of the deposited material or biomass.

1.2 Objective and scope of the project

The aim of the project is to design and develop a laboratory prototype of a thermal interferometer, which can be applied to testing of metals and coatings by a non-destructive inspection of the material. This device may be used to determine the diffusivity of different metals or it could be used to determine the thickness of a coating on a metal by measuring the phase lag created. This application could be developed further and would be very useful for measuring thickness and thermal properties of thermal barrier coatings.

Thermal interference can be measured using a surface temperature measuring device, usually a pyrometer. This method of measuring the thermal interference is more expensive

than the use of a microphone to measure the photo-acoustic effect. The aim is to measure the phase lag between interfering thermal waves to calculate the thickness or thermal diffusivity of a sample. The phase lag also depends on the reflection coefficient of the thermal waves and the phase lag introduced by converting the temperature variations at the surface of the sample into sound waves. A photo-acoustic cell may be illuminated from one side, or both sides of the sample. The standard one sided photo-acoustic cell suffers from an unknown phase lag, due to the microphone circuit and the phase lag introduced by the heat transfer from the sample surface to the gas in the photo-acoustic cell. Since the heat transfer conditions may vary with the sample and heat flux, a two sided photo-acoustic cell has been designed and used in the work reported here. The advantage of the two sided cell is that the unknown phase lags due to the acoustic part of the cell are eliminated. The experimental procedure developed for the two sided cell, illuminates both sides of the sample with the same frequency of modulated light. The phase shift of the modulation is altered to find a minimum response of the photo-acoustic cell. It is this minimum response phase shift that enables the thermal diffusivity or thickness of the sample to be determined. Since the measurement of a phase shift can be made very accurately, the method developed here might be used as a rapid and relatively cheap method for the accurate determination of thermal diffusivity or thickness of thin samples.

CHAPTER 2: LITERATURE REVIEW

2.1 History and background

The concept of thermal wave interference has been generated from the photo acoustic effect. In 1880, Alexander Graham Bell [1] discovered that when a periodically interrupted sunlight falls on a solid surface in an enclosed cell an audible sound could be heard by a hearing tube attached to the cell. Motivated by Bell's discovery Tyndall [3] and Rontgen [4] found that an audible sound is also produced when the chopped light passes through the cell filled with a gas. Subsequently, Bell experimented with a variety of gases, solids and liquids and created some interest in the photo acoustic effect.

After about fifty years, the photo acoustic effect became an established technique for gas analysis and is well interpreted; photons (the light particles) are absorbed by the gases and are converted into kinetic energy of gas molecules resulting in fluctuations within the cell leading to a production of acoustic signals.

In the mid seventies Rosencwaig and Gersho [2] observed the photo acoustic effect in solids and condensed matter leading to spectroscopic measurements, later known as photo acoustic spectroscopy. The theory given by them, predicts dependence of the acoustic signals on the absorption coefficient of the solid, thereby giving a theoretical foundation for the technique of photo acoustic spectroscopy. Based on this theory, optical absorption spectra can be obtained for optically opaque materials.

Later in 1981, Bennett and Patty [5] recast the Rosencwaig-Gersho [2] equation for the photo acoustic signals in such a manner which clearly emphasized the importance of thermal wave interference in the production of the photo acoustic signals. This formalism was used to extract thermal properties of many solids. The dependence of acoustic signals on chopped frequency was noticed, hence the technique adopted to extract the thermal information from structure of the material was to vary the wavelength of thermal waves by varying the frequency of modulated incident light and normalising the photo acoustic signal, which is done by using a signal from a thermally thick sample of the same material to remove the effects of cell resonances and the microphone response etc. In this way the structure revealed from thermal wave interference may be studied unambiguously, and the analysis of these data would yield the properties of the thermal waves and of the medium

in which they travel. This further supported the property of thermal waves being damped very quickly in the sample and thermal wave interference manifesting itself most predominantly in very thin thermal samples.

In 1987 Hasimoto, Cao and Takaku [8] dealt with the applications of photo acoustic effect for the measurement of thermal diffusivity in thin film samples. Also, the effect of sound wave interference inside the photo acoustic cell was observed and discussed. While studying thermal diffusivity and its measurements using the photo acoustic effect, they found that due to interference of thermal waves, an additional phase lag is observed between the resultant sound waves and the modulated incident beam. A theoretical expression has been developed between this phase shift and frequency of the modulated incident beam. Simulation results of the theoretical expression show good agreement with the experimental results. Furthermore some theoretical relations between the phase lag, the chopping frequency and thermal diffusivity of a sample have been reproduced following Rosencwaig-Gersho (R-G) theory.

In 2000, Cao [6], based on the Bennett and Patty [5] and R-G theory [2], extended the theory to cover the photo acoustic effect in multi-layered cells. The R-G theory accounts for the relationship between the temperature variation and the thermal properties for the front surface technique, which was expanded by Charpentier [7] to include the rear surface technique; however Bennett and Patty had formulated the thermal response as a superposition of thermal waves on the sample surface using interference theory and recast the RG theory.

Basically Cao in his mathematical formulation of the thermal response in a two layer photo acoustic cell, depicted the inter layer and intra layer interference of thermal waves explaining the origin of the phase lag in addition to an extra phase lag introduced due to thermal wave interference in various cases [6].

In Cao's experiment, a multi layered structure (glass window layer, sample layer and air layer) is placed in a PA (photo acoustic) cell. The thermal waves generated by a modulated light beam striking the front surface travel to and fro hitting the rear and front surfaces of the sample resulting in interference of the many reflections of the thermal waves. The periodical variation of temperature on the sample's surface leads to contraction and expansion of adjacent gas layers accordingly creating sound waves in the

cell. The sound output being detected by a sensitive microphone mounted on the rear side of the sample, is known as the rear surface technique. Normally the microphone is installed on the same side as incident beam of light, called the front surface technique.

The phase lag of the acoustic signal with respect to the modulated light signal is more useful in calculating the thermal diffusivity of a sample than acoustic amplitude. The total phase lag introduced between the sound signal and the chopped light signal is dominated by two components, one due to the travelling time of heat waves from one surface to the other surface of the sample and vice versa, and the other due to the delay in converting temperature fluctuations of the surface of the sample to sound waves that travel to the microphone. Thus the phase lags between the temperature variation on the surfaces of the sample and the modulated light may be termed as a 'thermal phase lag'; and the phase lag between temperature variation and the sound signal can be termed as, 'acoustic phase lag'. Though in a photo acoustic experiment the sum of the thermal phase lag and the sound phase lag is measured, Cao [6] and [8] addressed only thermal phase lag in his studies considering acoustic phase lag much lower compared to thermal phase lag due to long wavelength nature of acoustic waves.

It is the various techniques and theories of thermal wave interferometry carried out by earlier researchers that have led to the idea of developing and commissioning the two sided photo-acoustic cell to observe thermal wave interference in physical reality, which is the subject of this thesis.

2.2 Other approaches to this subject

a) Sensitivity of thermal-wave interferometry to thermal properties of coatings: application to thermal barrier coatings, Bendada 2004 [25]

In this paper the author has tried to estimate the sensitivity of thermal wave interferometry while applying it for the analysis of thermal properties of coatings. Several data sets were recorded from experiments on plasma sprayed yttrium-stabilized zirconia coatings to illustrate the accuracy and the limitations of thermal wave interferometry (TWI) for the evaluation of thermal properties of thermal barrier coatings.

It was found that this technique provides reliable thermal diffusivity values for larger values of the reflection coefficient but the best diffusivity measurements are possible for low values of reflection coefficient. And the characterization procedure is also influenced by signal to noise ratio. At low frequencies for thermally thick coatings accurate diffusivity

measurements are very difficult to make, but diffusivity can still be accurately determined. This is because TWI is very sensitive to effusivity at thin thermal thicknesses, and to diffusivity in the high thermal thickness region. The same was confirmed using three different thicknesses of coatings of plasma sprayed yttrium-stabilized zirconia on a copper substrate.

b) Theory of photo thermal-wave diffraction and interference in condensed media, Mandelis 1989 [15]

Mandelis has described thermal wave diffraction in condensed media deriving the thermal wave diffraction integral, thermal wave diffraction in the small aperture approximation and has explained photo thermal wave interferometry. He has presented several examples of photo thermal excitation apertures. These include the spatial impulse function, a Gaussian laser beam, a circular aperture, and an expression for the interference field generated by two Gaussian laser beams.

Thus a photo thermal wave diffraction formulation describing the temperature field dependence on arbitrary diffracting aperture geometries was developed and used to examine special cases of experimental importance, including source geometries leading to constructive or destructive thermal wave interference.

c) Photo thermal wave diffraction and interference in condensed media: experimental evidence Aluminium, Mandelis and Kwan 1991 [16]

In this study, using spatially resolved scanning by photo pyroelectric detectors, the optically generated thermal wave fields have been measured. Similar to Young's optical wave experiment thermal wave patterns have been produced by two laser beams interfering coherently, also diffraction profiles from a single laser beam have been produced. The diffraction and interference images have further been shown to be in excellent qualitative agreement with a Laplace thermal wave propagation formalism, which treats thermal wave diffraction in the small aperture approximation. A mechanism for quantitative agreement was obtained when the finite size of the metal detector tip was taken into account, in mapping thermal wave fields. A good agreement was found between photo pyroelectric experimental scans from thermally thick homogeneous aluminium sample of finite thickness and previously developed photo thermal diffraction and interference theory valid for semi-infinite solids.

d) Technique, application and noise analysis of purely thermal-wave photo pyroelectric Interferometry (PPEI), Mandelis and Wang 2001[17]

This is a new purely thermal wave interferometric technique which is based on spatial interference of thermal waves within the body of the pyroelectric transducer, independent of the sample. Unlike other conventional photo thermal interferometric schemes, this technique is based on monitoring thermal waves resulting from direct optical interference patterns, such as those generated by two appropriately modulated laser beams (for example intensity, phase or polarisation modulation). In the present coherence scheme thermal waves interfere as they are induced by two intensity modulated beams, split of a single laser source and with a fixed phase shift relationship between them. The usually large instrumental PPE (photo pyroelectric) baseline signal and a significant portion of the noise can be efficiently suppressed within the PVDF (polyvinyl dene fluoride) detector if the two laser beams are collinearly incident on opposite surfaces of the thin pyroelectric film, and with 180 degree relative phase shift. In this fashion, much higher signal sensitivity and dynamic range PPE measurements than with the conventional single beam PPE configurations are expected. This paper has presented a generalized theory of a purely thermal wave interferometry and applications which have been implemented for different research aspects including measurement of optical properties of solid laser crystals and the design and development of a novel H₂ gas sensor. In addition noise suppression and detectivity enhancement of the system is also discussed in this paper.

e) Thermal diffusivity measurement of polyethylene melt by a new temperature wave method, Hashimoto and Tsuji, 1993 [9]

This method used a new technique of measuring thermal diffusivity of high density polyethylene by a.c. Joule heating. The diffusivity was determined at various temperatures between room temperature and above the melting point in heating and cooling processes. This method also used the typical measurement of phase shift against the square root of frequency of temperature waves across the film sample.

It was found that the thermal diffusivity changed drastically at melting and crystallizing point at which obvious structural changes occurred. The main advantages of this method are: i) small temperature gradient, ii) wide temperature range including melt state, iii) small sample size ,iv) short measurement period and v) high resolution for temperature.

f) Thermal wave interferometry: a potential application of the photo acoustic effect, Bennett and Patty, 1982 [5]

This work was based on Rosencwaig-Gersho (R-G theory) [2], in which the equation for photo acoustic signal is a recast in a manner that emphasizes the crucial role played by thermal wave interference in the production of photo acoustic signals, as thermal wave interference effects manifest themselves most predominantly in samples that are very thin thermally. For this range of sample thickness and modulation frequencies, the thermo elastic stress waves are expected to contribute negligibly to the photo acoustic signals and hence the R-G theory was used as a foundation to this formalism by Bennett and Patty. They developed a theory and used it to suggest a technique for extracting thermal information from the structure in the photo acoustic signal resulting from thermal wave interference. It was stated that this technique is potentially a powerful and straightforward application of the photo acoustic effect in condensed phase.

CHAPTER 3: THEORY

3.1 Theoretical approach

3.1.1 Thermal Waves

The approach adopted here will be similar to that of Almond and Patel [26]. Heat is assumed to obey the diffusion equation within the sample:

$$\frac{\partial T}{\partial t} - \alpha \nabla^2 T = 0. \quad (1)$$

T is the temperature of the sample at point (x, y, z) at time t , with α being the thermal diffusivity of the sample. The boundary conditions at the surface of the sample are

$$Q = -k \nabla T, \quad (2)$$

where k is the thermal conductivity of the sample and Q is the heat flux entering or leaving the sample's surface.

In the one dimensional case, Equation (1) has solutions:

$$T = \{A \exp(-\sigma x) + B \exp(\sigma x)\} \exp(i \omega t), \quad (3)$$

where A and B are complex constants and ω is the circular frequency (radians per second) of the waves. The solution (Equation 3) looks like a propagating wave that is damped. It is usual to take the value of B to be zero for waves propagating in the positive x direction, as this ensures a finite solution as x tends to infinity. The value of σ is given by the dispersion relation for the diffusion equation:

$$i \omega - \alpha \sigma^2 = 0, \quad (4)$$

where σ is the wave number of the propagating thermal wave and is complex, meaning that the wave is damped:

$$\sigma = (1+i) \left(\frac{\omega}{2\alpha} \right)^{\frac{1}{2}}. \quad (5)$$

The expression for the complex wavenumber is often written as

$$\sigma = (1+i) \frac{1}{\mu}, \quad (6)$$

where μ is called the thermal diffusion length (a real number):

$$\mu = \left(\frac{2\alpha}{\omega} \right)^{\frac{1}{2}}. \quad (7)$$

Here α is the thermal diffusivity of the material and is given by $\alpha = \frac{\kappa}{\rho c_p}$, where ρ is the density, c_p is the specific heat capacity and κ is the thermal conductivity of the material.

Thus it can be seen that thermal waves decay to 1/e of their surface amplitude one thermal diffusion length below the surface. It is for this reason that some people are not comfortable with the oscillatory solutions of the diffusion equation as being wavelike. This is to some extent a question of semantics. If the system under consideration has length scales much shorter than the thermal diffusion length, then the damping is relatively small and the theory of scalar waves may be adapted to describing these solutions. In this sense, it is convenient to talk about “thermal waves”.

When light hits a surface and some is absorbed at the surface, then the absorbed light is converted to heat. Thus a modulated light source striking a surface acts as a modulated heat source. Using the boundary condition at the surface, it is easy to see the phase relationship between the thermal waves generated at the surface and the phase of the modulated light source.

Substituting the wave solution

$$T = A \exp(-\alpha x) \exp(i\omega t)$$

into the boundary condition (Equation 2), we find:

$$Q = -k\nabla T = k\sigma T = \frac{k}{\mu} A \exp\left(\frac{x}{\mu}\right) \exp\left(i\left[\omega t - \frac{x}{\mu} - \frac{\pi}{4}\right]\right)$$

$$\therefore Q = \frac{k}{\mu} T \exp\left(-i\frac{\pi}{4}\right) \quad (8)$$

Thus a phase difference of 45° exists between the modulated light and the temperature waves at the surface of the specimen. This phase difference is in addition to any phase lag that might occur when converting the temperature fluctuations at the surface into sound waves.

3.1.2 Sound wave generation by thermal waves

In the photo-acoustic cell shown in Figure 3.1 light passes through the transparent window

and strikes the sample on the far side of the cell. The cell is gas tight and the microphone responds to pressure changes caused by the gas being heated and cooled by the sample surface. The heat flux arriving at the surface will have the form $Q_{\exp}(i\omega t)$. In the equations below the time variation will be dropped for clarity.

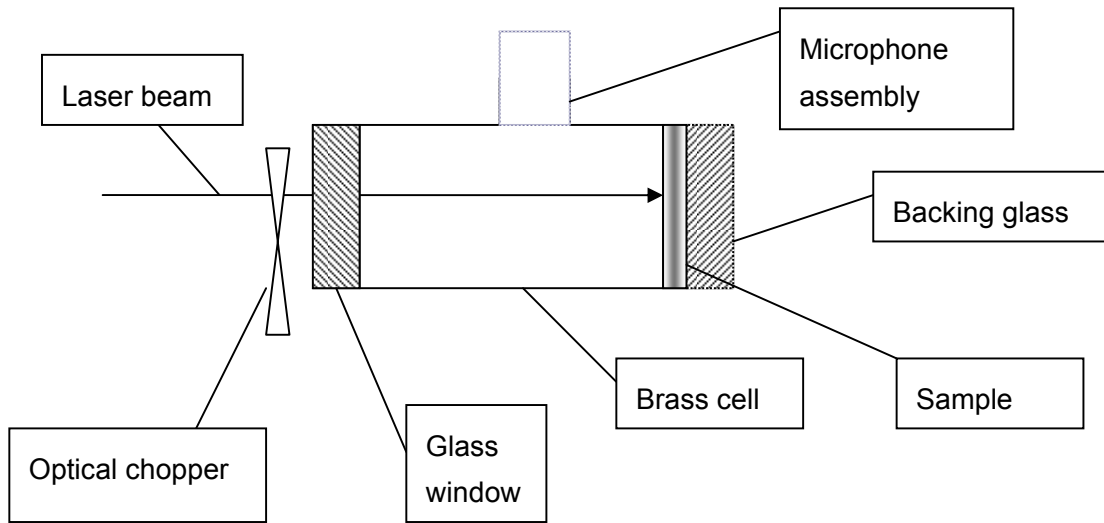


Figure 3.1 Schematic diagram of a simple photo-acoustic cell

The temperature difference between the surface of the sample and the gas in the cell will cause the gas in the cell to heat up. The heat flux being absorbed by the gas from the surface of the sample can be written

$$Q_{gas} = H(T - T_{gas}), \quad (9)$$

where T_{gas} is the bulk gas temperature (not the boundary layer next to the surface of the sample) and H is the heat transfer coefficient. As the bulk of the gas heats up, so its temperature will rise according to

$$Q_{gas} = mc_v \frac{\partial T_{gas}}{\partial t}, \quad (10)$$

where m is the mass of the gas enclosed in the cell and c_v is the specific heat of the gas at constant volume. Heat loss from the gas to the cell's walls has been ignored. Since the system is being driven at frequency ω , Equation (10) becomes:

$$i\omega mc_v T_{gas} = H(T - T_{gas}), \quad (11)$$

which means that the bulk gas temperature can be expressed in terms of the sample's surface temperature.

$$T_{gas} = \frac{T}{(1 + i\omega\tau_{gas})}, \quad (12)$$

$$\text{where } \tau_{gas} = \frac{mc_v}{H}. \quad (13)$$

It is very likely that the time constant τ_{gas} associated with converting the sample's surface temperature into sound waves will depend on the frequency and the amplitude of the surface temperature fluctuations, as well as the mean temperature of the surface. This is because the convection cell set up in the cell will be driven by natural convection (gravity). Thus the boundary layer thickness that dictates the Nusselt number and therefore the heat transfer coefficient will depend on the period of the oscillation as well as its amplitude. The amplitude dependence comes about because the modulated light beam does not cool the sample in the negative part of the cycle, but consists of a fluctuating component plus a mean value. The mean value (or zero frequency) heat flux will drive the convection cell, thus the larger the amplitude of the modulated light beam, the larger the mean temperature difference between the gas and the sample's surface. In natural convection, the higher the temperature difference, the greater the heat transfer coefficient.

Consider the perfect gas law

$$P = \frac{nR}{V} T_{gas}. \quad (14)$$

The volume of the gas is constant and so the relationship between the gas pressure and the heat flux from the modulated light beam can be derived using Equation (8) and (12).

$$\begin{aligned} Q &= -k\nabla T = \frac{k}{\mu} T_{gas} (1 + i\omega\tau_{gas}) \exp\left(-i\frac{\pi}{4}\right) \\ \therefore Q &= \frac{k}{\mu} \frac{PV}{nR} (1 + i\omega\tau_{gas}) \exp\left(-i\frac{\pi}{4}\right) \end{aligned} \quad (15)$$

This leads to the phase relationship between the pressure of the gas (sound picked up by the microphone) and the modulated light incident on the sample's surface.

$$\frac{P}{Q} \propto \frac{1}{(1 + i\omega\tau_{gas})} \exp\left(i\frac{\pi}{4}\right) \quad (16)$$

Equation (16) has two obvious limits. At very low frequency $\omega\tau_{gas} \ll 1$, the phase lag

between the sound and the modulated light will be 45° and at high frequencies $\omega\tau_{gas} \gg 1$, the phase lag between the sound signal and the light will tend to 135° .

A more sophisticated model of the generation of the sound is possible, but this simple model seems to encapsulate the most important feature. That is the added phase lag in producing the sound. It is this uncertainty in the knowledge of the gas time constant τ_{gas} that means that any measurements of phase lag on a single sided cell (Figure 3.1) will need to be calibrated against a standard that reproduces the same phase lag associated with the generation of sound.

3.2 Theory of a single sided photo acoustic cell

Using the wave analogy as described in Section 3.1, the thermal wave interference for a single sided photo thermal cell can be described as follows:

A thermal wave (primary wave, W) is generated instantaneously as soon as a modulated light impinges on the front surface of the sample in substrate form (S_{12} in Figure 3.2). The thermal wave travels towards the rear surface of the substrate (S_{23} in Figure 3.2), reflects and arrives on the front surface again, forming the so called secondary wave. The travelling and reflecting back process of the thermal wave continues between both surfaces S_{12} and S_{23} until it is damped completely. The temperature variation on the front surface is the superposition of the primary, secondary and higher waves (Figure 3.3). While there is no phase lag between the primary wave and the modulated light given that the time for energy conversion from light to heat is less than 10^{-9} second [6], there is a phase lag existing between the modulated light and the overall temperature variation on the surface S_{12} as expressed in Equation (8).

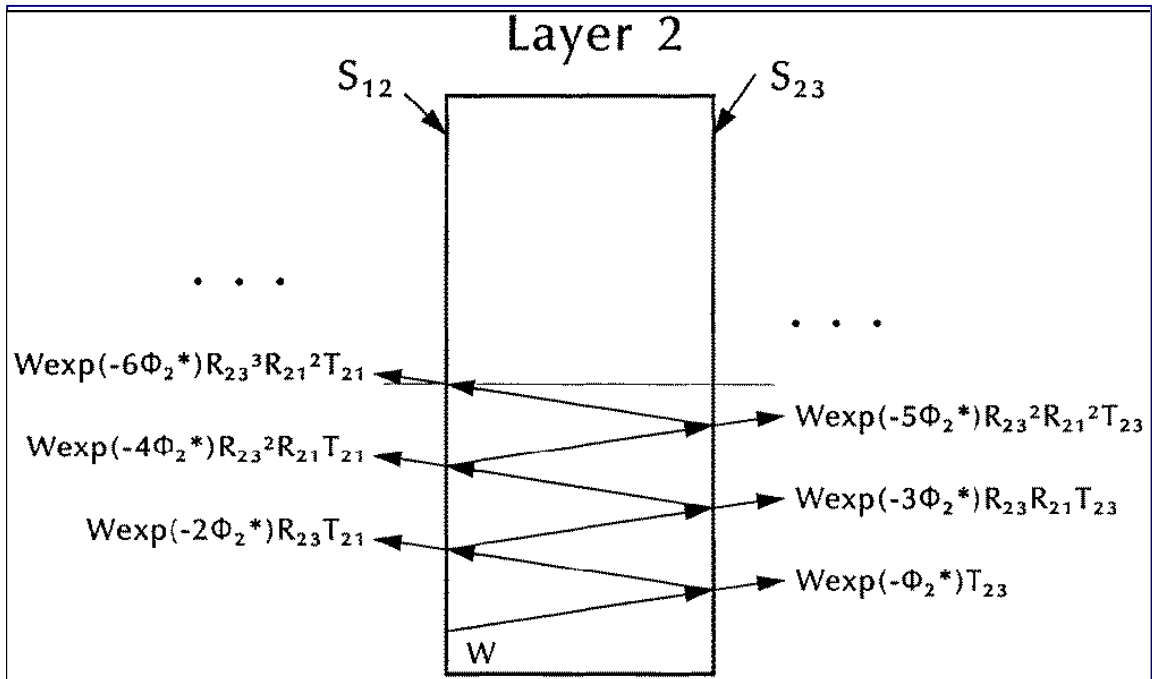


Figure 3.2 Superposition of thermal waves [6]

Note: Φ is written as φ in Section 3.2.1 for convenience.

3.2.1 Interpretations of the thermal phase lag in the front-surface technique

The temperature variation on the front surface of the substrate has been formalized by Cao [6]. For the front-surface technique, by considering layer 1 as an air layer and assuming it to be thermally thick, the interference effect from the thermal waves reflected from the interface, S_{01} , can be neglected. Summing up all of the thermal waves on the front surface of the sample, which form a geometric series, leads to the expression of the temperature variation on the front surface of the sample

$$I = T_{21} R_{23} \frac{1}{1 - R_{23} R_{21} \exp(-2\varphi_2^*)}, \quad (17)$$

where:

I is the total intensity at the front surface.

$$R_{ij} = \frac{1 - b_{ij}}{1 + b_{ij}} \quad \text{---- Reflection coefficient}$$

$$T_{ij} = 1 - R_{ij} \quad \text{---- Transmission coefficient}$$

$$b_{ij} = \frac{e_j}{e_i} \quad \text{----- Ratio of effusivities}$$

$$e = \sqrt{\rho \cdot c_p \cdot \kappa} \quad \text{-----Effusivity}$$

where ρ , c_p and κ are the density, heat capacity and thermal conductivity of the gas layer, respectively.

φ_2^* represents the complex thermal diffusion length and is given by

$$\varphi_2^* = (1+i)\varphi_2 = (1+i) \sqrt{\frac{\omega}{2\alpha_2}} l_2, \quad (18)$$

where ω is the modulation frequency of the light source, and α_2 and l_2 are the thermal diffusivity and the thickness of layer 2 (the substrate), respectively.

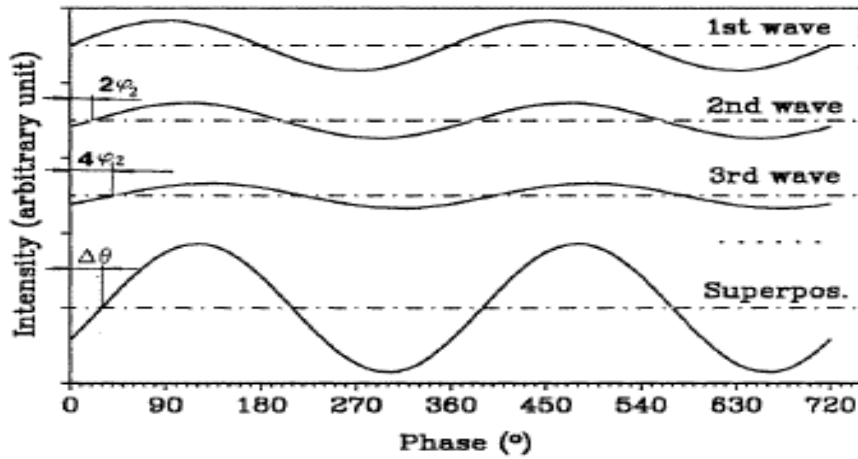


Figure 3.3: Schematic showing how the superposition generates an additional phase lag $\Delta\theta$ in the front surface of the sample [6]

The above explanation can be further illustrated by using Figure 3.3 and by explicitly defining the various contributions to the total observed phase lag φ_T between the optical and acoustic signals:

$$\varphi_T = \varphi_{pt} + \varphi_{ia} + \Delta\theta,$$

where φ_{pt} is the “photothermal” phase lag (equal to 45° according to Equation (8)), φ_{ia} is the “thermoacoustic” phase lag (defined by Equation (16)) and $\Delta\theta$ is an additional “thermal interference” phase lag due to the interference between the primary, secondary and higher thermal waves. The first thermal wave, which is generated upon the absorption of the modulated light by the sample, should have no thermal interference phase lag due

to interference of thermal waves. It is the second thermal wave and the higher waves that show the phase lags ($2\varphi_2, 4\varphi_2, \dots$) after their multiple travels between the interfaces, S_{12} and S_{23} .

The temperature variation on the surface of a sample is the superposition of the first, second and higher thermal waves. The origin of the thermal interference phase lag ($\Delta\theta$) in a front-surface arrangement lies in the intra-layer interference effect. Thus for a thermally thick sample, the second and higher waves are so damped that little contribution to the superposition could be anticipated. The thermal interference phase lag approaches zero. Similarly, as the modulation frequency ω increases, the thermal diffusion length μ decreases according to Equation (7) and the thermal interference phase lag for the front-surface technique will tend to zero.

3.3 Theory of a double sided photo acoustic cell

To explain the phenomenon of thermal interference in a double sided photo acoustic cell, the mathematical treatment below has been developed.

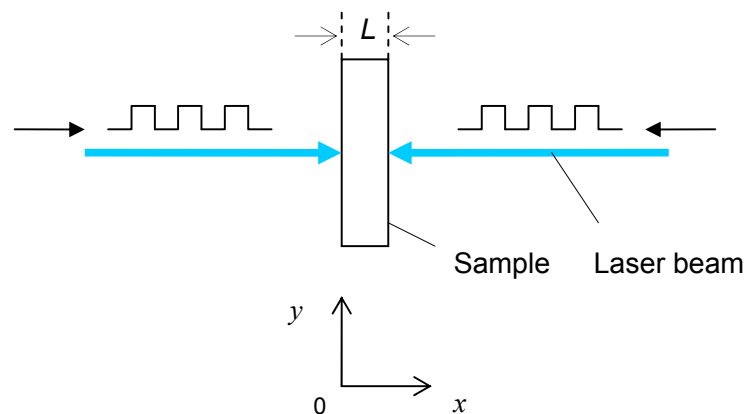


Figure 3.4 Schematic diagram for a double sided cell system

The problem is to determine the response of a thin planar sample irradiated on either side by modulated laser beams of (roughly) equal intensity. The area irradiated has a diameter greater than the sample thickness (L), so we shall treat the sample temperature as a

function of one spatial variable (x) only. The boundary conditions are assumed linear and time-invariant, so that the system as a whole is LTI, and we can solve for each of the Fourier components of the temporal response independently, at least in the steady state. Outside the sample the 1-D approximation will break down for the DC component, but should be reasonably accurate for time-varying components; we shall assume so for now at any rate.

If the thermal flux density at x at time t is $\mathbf{J}(x,t)$, and $U(x,t)$ is the corresponding thermal energy density, then, for $0 < x < L$

$$\nabla \cdot \mathbf{J}(x,t) + \frac{\partial U(x,t)}{\partial t} = P(x,t), \quad (19)$$

where $P(x,t)$ is the density of power absorbed from the laser beam. The usual assumptions:

$$\mathbf{J}(x,t) = -k\nabla T(x,t) \quad (20)$$

and

$$U(x,t) = \rho c_p T(x,t) \quad (21)$$

(which should be valid, at least for small perturbations about the DC values), lead to the well known heat flow equation, which forms the effective starting point of our analysis:

$$-k\nabla^2 T(x,t) + \rho c_p \frac{\partial T(x,t)}{\partial t} = P(x,t). \quad (22)$$

Suppose the laser modulation is periodic, so that

$$P(x,t) = \sum_n P_n(x) e^{i\omega_n t} \quad (23)$$

and, in the steady state,

$$T(x,t) = \sum_n T_n(x) e^{i\omega_n t} \quad (24)$$

gives the temperature distribution. The equation for the n^{th} harmonic is

$$-k \frac{d^2 T_n(x)}{dx^2} + i\omega_n \rho c_p T_n(x) = P_n(x). \quad (25)$$

Now define

$$\alpha_n = (1+i) \sqrt{\frac{\omega_n \rho c_p}{2k}} \quad (26)$$

where α_n the complex wave number is associated with the thermal diffusivity α at frequency ω_n and is given by $\alpha_n = (1+i)\sqrt{\frac{\omega_n}{2\alpha}}$. Then, in the region $0 < x < L$, the general solution to Equation (25) can be written in the form

$$T_n(x) = A_n e^{-\alpha_n x} + B_n e^{\alpha_n x} + \theta(x)$$

$$\theta(x) = \frac{1}{2\alpha_n k} \int_0^L e^{-\alpha_n |x-x'|} P_n(x') dx' \quad (27)$$

If the sample is a good conductor, then we should be able to write

$$P_n(x) = \frac{1}{\delta} \left(P_{0n} e^{-\frac{2x}{\delta}} + P_{1n} e^{-\frac{2(L-x)}{\delta}} \right), \quad (28)$$

where δ is the penetration depth of radiation at the laser wavelength and P_{0n} and P_{1n} are proportional to the n^{th} Fourier components of the modulated laser intensity incident on the $x = 0$ and $x = L$ surfaces respectively.

The integral in (27) is easily evaluated. For convenience define:

$$h_n(x) = \frac{1}{2\alpha_n k \delta} \int_0^L e^{-\alpha_n |x-x'|} e^{-\frac{2x'}{\delta}} dx'$$

$$= \frac{\delta e^{-\left(\frac{2}{\delta}\right)x}}{k((\alpha_n \delta)^2 - 4)} - \left(\frac{e^{-\alpha_n x}}{2k\alpha_n(\alpha_n \delta - 2)} + \frac{e^{-\alpha_n(L-x)} e^{-\left(\frac{2}{\delta}\right)L}}{2k\alpha_n(\alpha_n \delta + 2)} \right) \quad (29)$$

In terms of $h_n(x)$ Equation (27) becomes

$$T_n(x) = A_n e^{-\alpha_n x} + B_n e^{\alpha_n x} + P_{0n} h_n(x) + P_{1n} h_n(L-x) \quad (30)$$

The constants A_n and B_n are determined by the boundary conditions at $x = 0$ and L . For the DC term, $\omega_0 = 0$, these are likely to be complicated since the solution of the heat conduction equation in the outer region results in linear x dependence, and the $|x| \rightarrow \infty$ conditions are essentially undetermined. In reality the 1-D approximation must fail on the outer region and this would take us beyond the simple model. Fortunately the non-DC terms have non-zero frequency and the solutions are exponential in x and the natural non-DC condition at infinity, $T_n(\pm\infty) = 0$, leads to plausible 1-D solutions. Also, the low thermal

conductivity of the surrounding air suggests that a null flux condition at $x = 0$ and $x = L$ may be adequate for the oscillating component. This may be preferable as an approximation since the actual coupling at 0 and L may not be correctly modelled as simply conductive.

In any event we shall assume that a simple matching of conductive heat fluxes across the boundaries is sufficient for now, and will usually take the limiting null-flux conditions for analytical calculations.

Thus if the thermal conductivity of the outer region is k_0 , and the other outer medium quantities are similarly subscripted, then the boundary conditions at $x = 0$ and L become

$$T_0(x) = T(x) \text{ when } x = 0, L \quad (31)$$

and

$$-k_0 \frac{\partial T_0}{\partial x} \Big|_{x=0,L} = -k \frac{\partial T}{\partial x} \Big|_{x=0,L} \quad (32)$$

where

$$T_0(x) = \begin{cases} T(0)e^{\alpha_{0n}x} & ; x < 0 \\ T(L)e^{-\alpha_{0n}(x-L)} & ; x > L \end{cases} \quad (33)$$

and (27) and (31) have been used with $P = 0$, together with $T_n(\pm\infty) = 0$ to determine the outer solutions.

Substituting for T and T_0 in Equation (32) at the two boundaries yields

$$\begin{bmatrix} -\left(1 + \frac{\alpha_{0n}k_0}{\alpha_n k}\right) & \left(1 - \frac{\alpha_{0n}k_0}{\alpha_n k}\right) \\ -\left(1 - \frac{\alpha_{0n}k_0}{\alpha_n k}\right)e^{-\alpha_n L} & \left(1 + \frac{\alpha_{0n}k_0}{\alpha_n k}\right)e^{\alpha_n L} \end{bmatrix} \begin{bmatrix} A_n \\ B_n \end{bmatrix} = \begin{bmatrix} \frac{-1}{\alpha_n} \theta'(0) + \frac{\alpha_{0n}k_0}{\alpha_n k} \theta(0) \\ \frac{-1}{\alpha_n} \theta'(L) - \frac{\alpha_{0n}k_0}{\alpha_n k} \theta(L) \end{bmatrix} \quad (34)$$

This is easily solved for A_n and B_n .

Note that in practice $\frac{\alpha_{0n}k_0}{\alpha_n k} \ll 1$ and the penetration depth δ is also very small. In the limit

in which these two terms are taken to zero it can be shown (after some tedious but straightforward algebra) that at $x = 0$

$$T_n(0) = P_{0n} \frac{(\cosh(\alpha_n L) + r e^{i\phi})}{2\alpha_n k \sinh(\alpha_n L)} \quad (35)$$

$$\text{where } re^{i\phi} = \frac{P_{1n}}{P_{0n}}. \quad (36)$$

The phase lag, ϕ (more precisely called a 'laser phase shift', which is the phase difference observed between the two incident laser beams on the sample from opposite directions) at which the amplitude of the fundamental of the temperature variation is a maximum or minimum, can be derived from Equation (36), and maximum phase lag is given by

$$\tan \phi_{\max} = \tanh(\gamma L) \tan(\gamma L), \quad (37)$$

$$\text{where } \gamma = \sqrt{\frac{\omega \rho c_p}{2k}} \quad (38)$$

This is the same result as quoted in Almond and Patel's book on page 211 [26].

It is important to note how accurate the measurements would be for a given error in determining the phase shift. In the double sided photo acoustic cell, it is preferable to find the minimum in the temperature variation by measuring the minimum amplitude of the acoustic signal, as the maximum acoustic amplitude is varying slowly. The laser phase lag for which the temperature variation is a minimum is related to the maximum phase lag by the relationship

$$\phi_{\max} = \phi_{\min} + \pi. \quad (39)$$

The measurement of the minimum amplitude starts at 180°, when the product γL tends to zero. The measurement then apparently decreases from 180° as the frequency rises or for thicker samples. A plot of the solution to Equation 37 is shown in Figure 3.5.

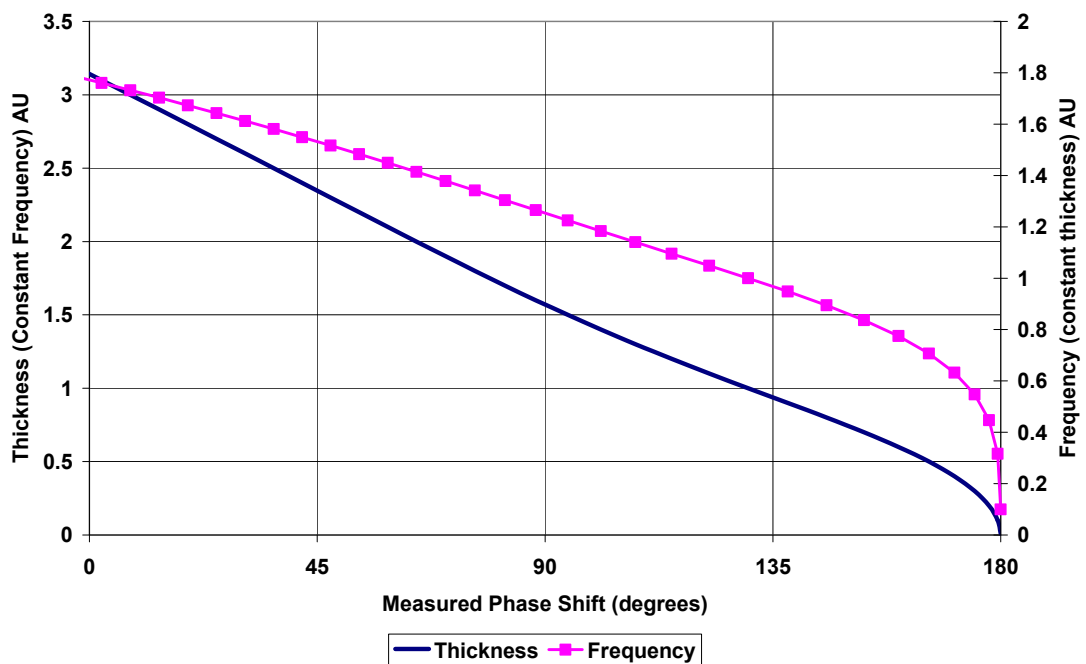


Figure 3.5 Shape of the measured laser phase shift for the minimum amplitude of the temperature variation in a double sided cell

For the convenience of the reader, Figure 3.5 is split into two charts: Figure 3.6a shows the variation of the laser phase shift plotted against the laser modulation frequency when the thickness of sample is constant, while Figure 3.6b shows the variation of the laser phase shift plotted against the thickness of the sample when the modulation frequency is constant.

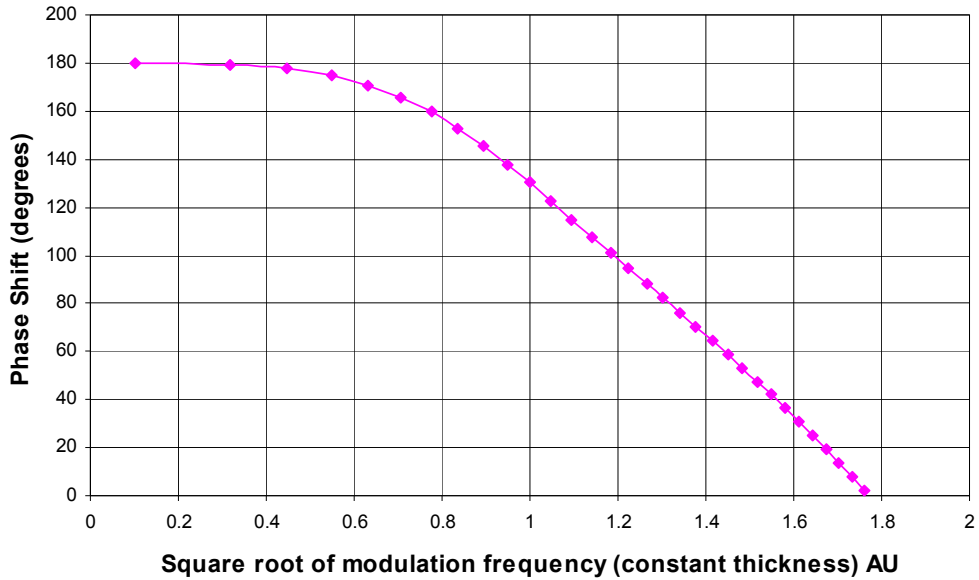


Figure 3.6a Phase shift variation against modulation frequency (constant thickness)

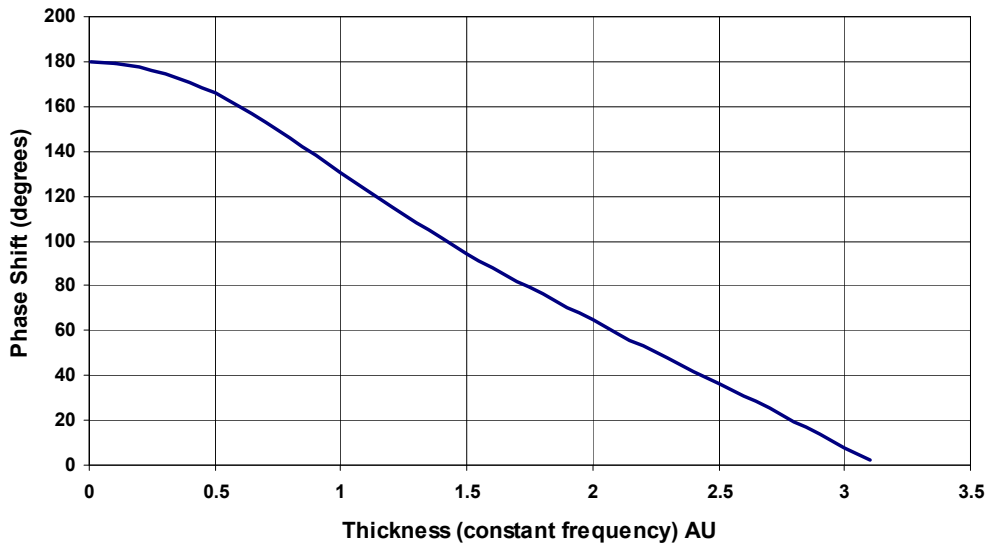


Figure 3.6b Phase shift variation against thickness of sample (constant frequency)

Figure 3.6b helps us to see a physical explanation for the dependence of the signal minimum on sample thickness. For a sample of zero thickness a signal minimum is expected when the laser beams on the two sides of the sample are 180° out of phase.

When the sample has a finite thickness, the minimum temperature variation occurs when the thermal phase lag through the sample plus the laser phase lag equals 180°.

The measurement of phase will have an error independent of the value. So the error in measuring the product γL will depend on how accurately the phase shift can be measured.

From Equation (37) it is easy to show that:

$$\delta(\gamma L) = \delta\phi_{\min} \frac{(\tanh^2(\gamma L) - 1)(\tan^2(\gamma L) - 1)}{\tanh^2(\gamma L)\tan^2(\gamma L) + 1} \quad (40)$$

where δ represents the error in the measurements. Figure 3.7 shows Equation (40) plotted out as a percentage error in γL for an error in the phase measurement of one degree.

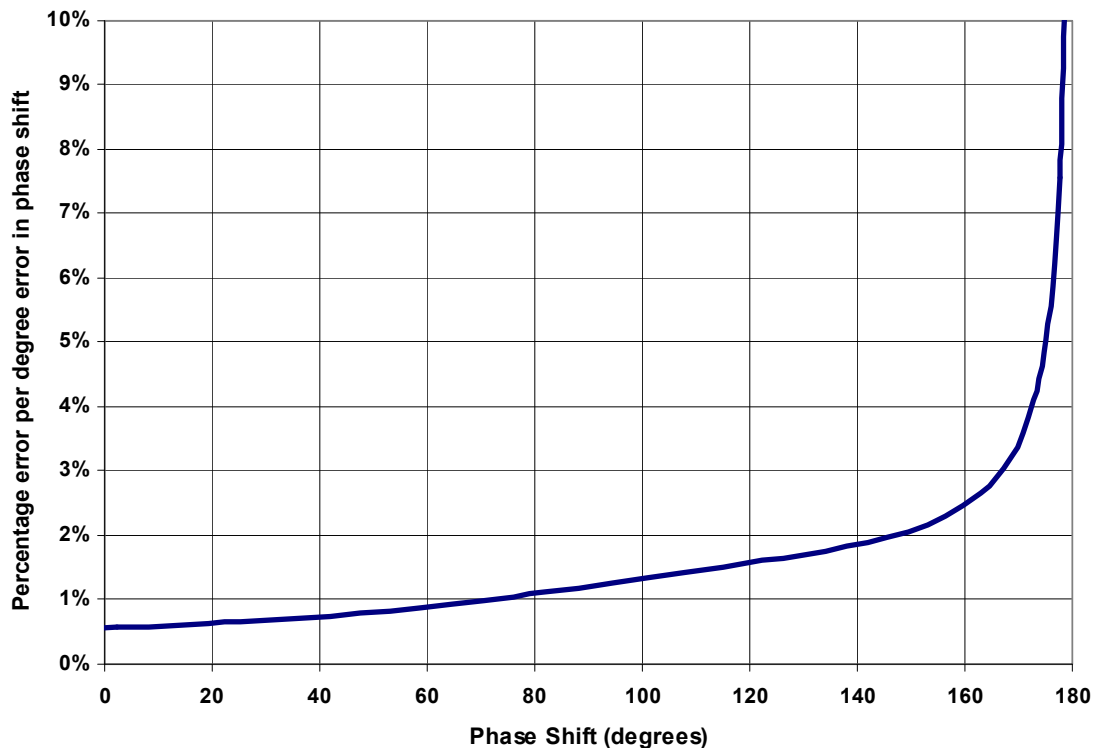


Figure 3.7 Percentage error γL per degree error in phase shift for a double sided cell

This shows that the largest errors will occur in the thinnest samples at low frequencies. The further the phase shift is from 180°, the smaller the error. Figure 3.7 shows that for a one degree error in phase shift measurement, errors in measurement of γL will be less than one percent provided the measured phase shift is less than about 80° (that is the phase shift is greater than 100° from 180° that would be experienced by an infinitely thin

sample).

The above discussion suggests that the thermal interference effect in a double sided photo acoustic cell can be used to study the thickness and thermal properties of thin samples, while avoiding the complicating factor of the thermoacoustic phase lag φ_{ta} , as defined by Equation (16). The exact phase lag between the modulated laser beams and the acoustic signal is not required in this approach, as we are only interested in the amplitude of the acoustic signal as a function of the phase difference ϕ between the two laser beams.

CHAPTER 4: CONSTRUCTION OF A LABORATORY THERMAL WAVE INTERFEROMETER

To make a thermal interferometer we have considered the superposition of thermal waves when the sample is irradiated from both sides, front and rear, by two modulated laser beams obtained by splitting a single laser beam using a 50/50 beam splitter. These two beams are synchronised at the same frequency by locking an acousto-optic modulator (beam1) to the reference of an optical chopper (beam2). A variable phase shift ϕ is introduced between the two beams relative to each other by moving the same chopper blade (cutting the beam orthogonally) in the path of the beam. Thus a phase difference ϕ referred to as the 'laser phase shift' is created between these two split beams, which leads to a similar phase lag between the resultant thermal waves inside the sample and their interference effect is observed through recording the amplitude of the resultant photo acoustic signals.

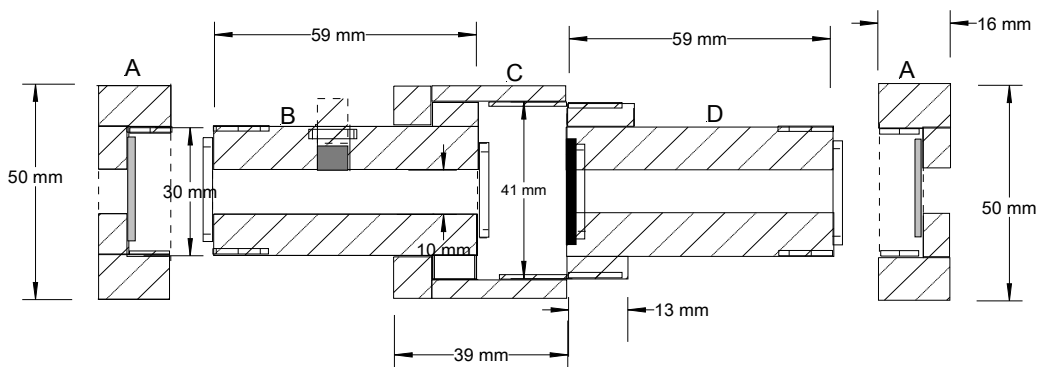
Here it is necessary to describe the photo-acoustic technique in short as adopted by us in the current work. In this technique, an intense beam of light, interrupted at regular intervals is incident on a metal sheet of micron level thickness through a glass window, inside an airtight enclosed cell. The light energy incident on the surface is converted into thermal energy which propagates through the metal sheet. This results in an increase in temperature of the metal surface and hence the adjacent layer of air. Due to the temperature rise, the air (or gas) inside the cell expands but as the volume of the cell is fixed, it creates a pressure inside the cell following the ideal gas law ($PV = nRT$), which in turn generates acoustic signals in the range of a few decibels. These acoustic signals are captured by a sensitive microphone and fed to the diagnostic electronics for recording and further analysis. The experimental details will be described in following Sections. A simple pictorial representation is already given in Figure 3.1 for a single cell system irradiating the sample from one side only. However in this project a double sided photo acoustic cell has been used and we will now describe its design and details.

4.1 Design and drawing of photo acoustic cell

We designed a special photo acoustic cell to meet our experimental requirements. A detailed drawing using the software "Auto Sketch" was prepared as shown below in

Figures 4.1 and 4.2. The photo acoustic cell (PA Cell) is the heart of the thermal interferometer and its design and construction was very important for the success of the experiments. To construct this cell, brass was selected as a material as it was easy to machine and was suitable for this design and purpose. From the sketch shown in Figure 4.1, separate designs for all parts of the cell were worked out and then a solid piece of brass was machined in the workshop as per detailed specifications within a tolerance of $\pm 1\text{mm}$. Most important was to make the cell air tight with the flexibility of replacing samples at times. So we used several rubber O-rings and designed the parts so that they can hold together tightly. Also to minimise scattering of light, inner surfaces were blackened by an oxidation process.

Cell Assembly Drawing



The dimensions shown here are approximately (tolerance of $\pm 1\text{mm}$) same as of the actual cell

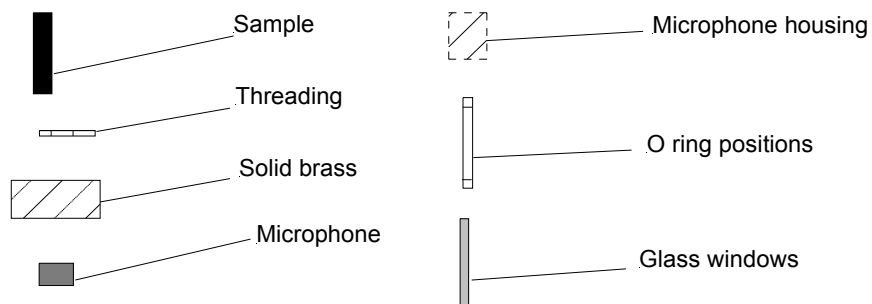


Figure 4.1 Diagram of a two sided photo-acoustic cell

The photo acoustic cell components drawings are shown in Figure 4.2.

Parts Drawing

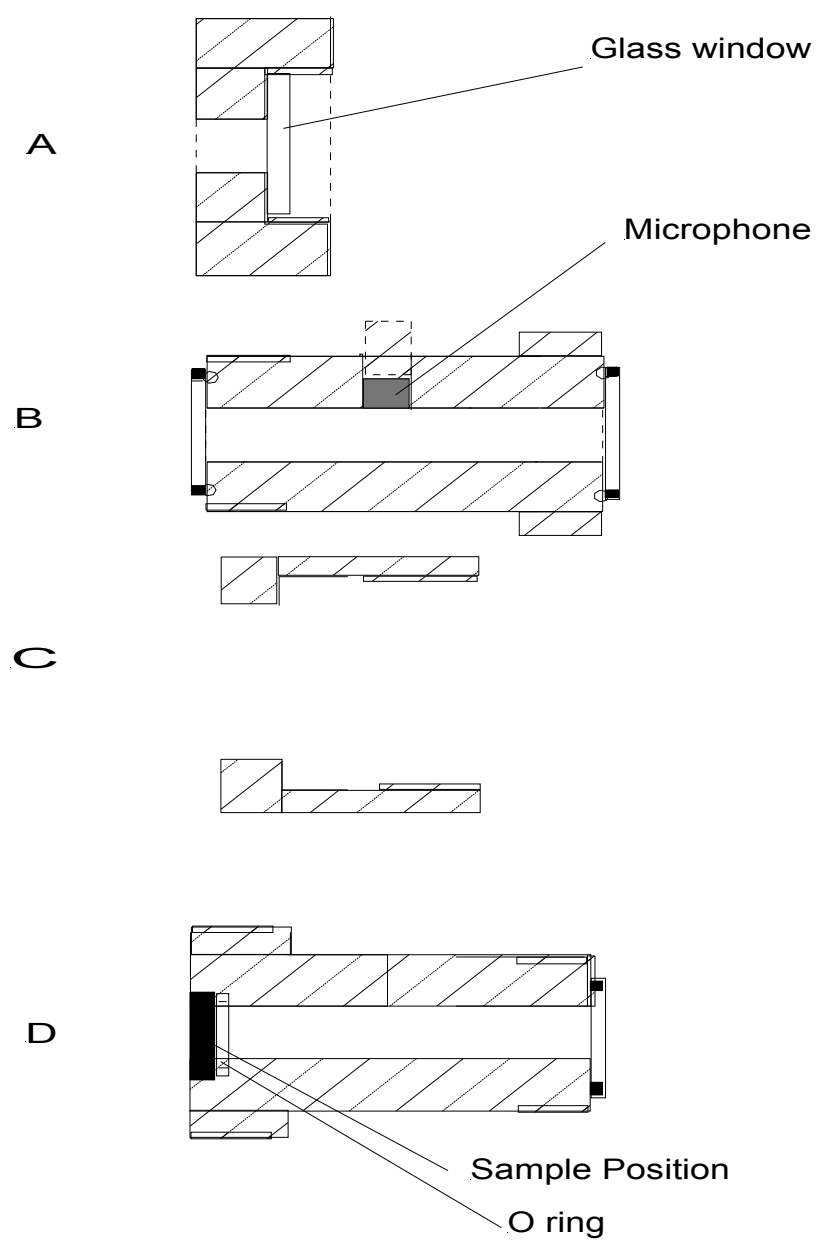


Figure 4.2 Diagram of two sided photo-acoustic cell components

1. The PA cell contains four parts, A, B, C and D.
2. There are two of part A and one each of part B, C and D. The parts A are at both ends facing each other, however B, C and D are in the middle in a row. Part A can be connected to parts B and D from two ends, however part C slides on B and works as a coupler to join B and D. All the four parts A, B, C and D are made of solid brass in a cylindrical form with circular hole of same diameter approx. 10mm as shown. All the parts have threading to tighten to each other. Other dimensions are also shown in the drawing 4.2. An photograph showing the cell assembly (Figure 4.5) is shown in Section 4.3.
3. Part A has a slot to take up a circular glass window which is to be glued on the circular annular surface against the hole.
4. Part B has a circular groove at each end on which rubber O-rings are fitted. It also has a hole drilled from side wall to fix a sensitive microphone. One end of part B, which joins with D, has actually larger external diameter, which is meant to hold part C, so that C and D can be tightened to join B and D. Further, parts B and D have grooves for O-rings to make it air tight with parts D and A. The other end (left end) of part B joins with A through the threading.
5. Part D is similar to B, but its outer front face joins with the inner front face of part C. Part D also has a slot facing B to accommodate the sample, which is a circular substrate of copper. The other end (right end) of part D joins with another part A with the threading.
6. Thus all the four parts A, B, C and D join each other with the threading and make it an air tight photo acoustic cell.
7. The samples consist of pure copper discs with a diameter of 14mm and thickness varying from 100 μm to 3 mm.
8. The glass windows consist of ordinary glass of diameter 14mm and thickness 2mm.
9. The O-rings are approx. 12-14 mm in diameter with a thickness of 1-3 mm matching the grooves on the blocks.

4.2 Components and equipments for construction of thermal interferometer

To perform experiments the following main components were selected:

- a) A photo acoustic cell of brass as shown earlier was designed and constructed and was blackened on the inside by an oxidation process.
- b) A dual input phase sensitive lock-in amplifier from Stanford Research Systems, SR530 was used with mechanical optical chopper SR540. This lock-in amplifier has the ability to measure amplitude and phase of a locked in signal simultaneously and hence was quite a useful tool.
- c) The optical chopper SR 540 was also used on a translation stage to introduce a phase shift ϕ in one laser beam relative to the other. The chopping blades used were of 6 slots and 30 slots, which were capable of producing a frequency range of 4 Hz to 400 Hz and 400 Hz to 3.7 KHz, respectively.
- d) A Tektronix oscilloscope was used to record and observe data.
- e) A prepolarised $\frac{1}{2}$ " diameter pressure diffused microphone 40AD with a preamplifier 26CA from 'G.R.A.S. Sound and Vibration', Denmark was used. The sensitivity of this microphone is mV/Pa, dynamic range is 17 to 146dB, resolution 20 μ Pa, and frequency range is 6.3 Hz to 10 KHz.
- f) An air cooled argon-ion gas laser model 163D-02 from Spectra Physics, USA with multiple line output (488 nm prominent) was used. Initially, two He-Ne lasers of 10 mw and 632.8 nm from Aerotech Inc., USA were used.
- g) An acousto optic modulator AOM-40 (from Intra Action Corp., USA) with light modulator signal processor ME-40, a photo-diode detector, plane mirrors, a 50/50 beam splitter, translation stage and various mounting posts were also used.
- h) The entire set up was made on a vibration isolation optical table from Newport Corporation, USA.

4.3 Experimental set up and circuit diagram

The following system design was worked out after several considerations and preliminary experiments. The complete experimental set up was laid down on a suitable vibration isolated optical table.

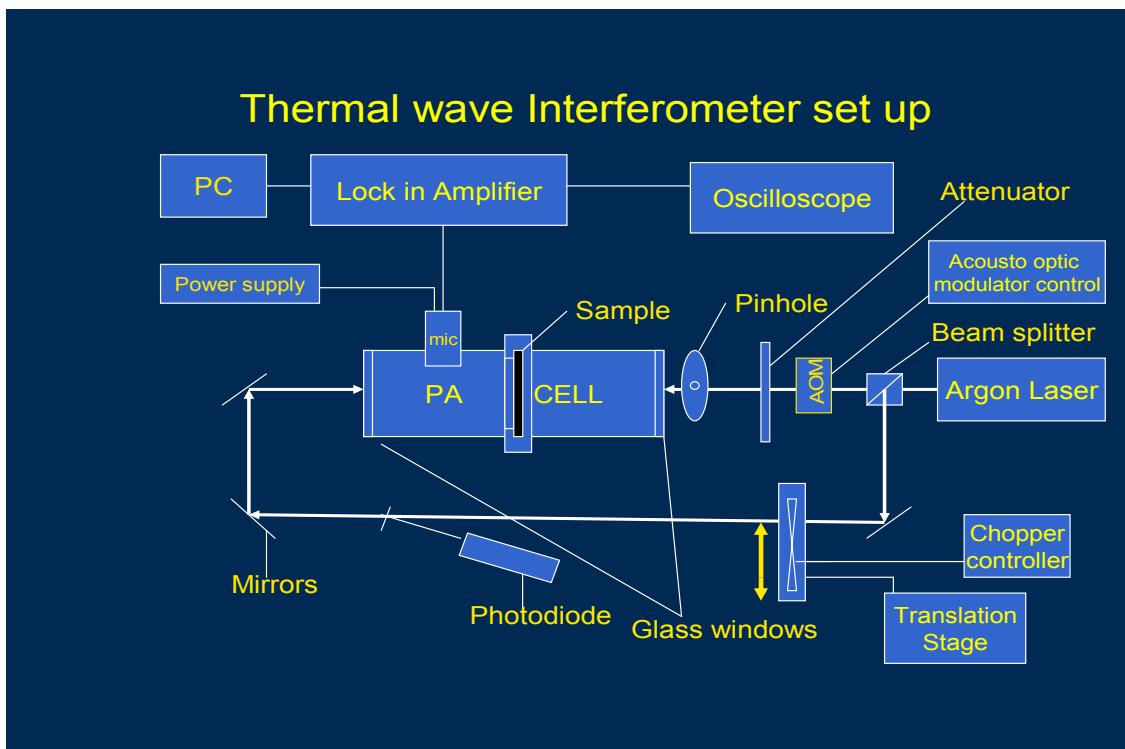


Figure 4.3 Thermal wave interferometer set up

The components shown in Figure 4.3 were connected by BNC cables and power line as per Figure 4.4.

In this set up an intense laser beam of mixed frequency (488 nm prominent) from an argon-ion laser was split by a 50/50 beam splitter and allowed to fall on the sample inside the PA cell from two opposite directions after passing through steering plane reflecting mirrors and other optical components as shown in the Figure 4.3.

An acousto-optic modulator (AOM) was used to modulate the front beam driven by the reference frequency from the optical chopper (on the split beam) to the AOM controller.

Thus we could obtain perfect frequency synchronisation on both beams and could verify it on a digital oscilloscope as well. Further, using a photo detector on the split beam, we could easily measure the phase of the beam falling on the sample from the front. The waveform generated by the rear beam is also recorded by the oscilloscope and the phase difference ϕ between the two waveforms was easily measurable. This phase difference between two beams can be varied by moving the chopper blade on the linear translation stage. Thus it was possible to introduce a desired phase shift of one beam with respect to the other. A variable optical attenuator was used on the main beam path going straight to the cell to attenuate the laser power and hence balancing the beam power with the split beam. This is useful in controlling the laser power falling on the sample from both sides equally. This is done by measuring laser power using a 'Coherent' laser power meter at both ends of the cell just before the glass windows. A pinhole is also used to pass only the first order diffracted beam from AOM and cutting of zero, second and third order beams.

Thermal wave Interferometer Schematic Diagram

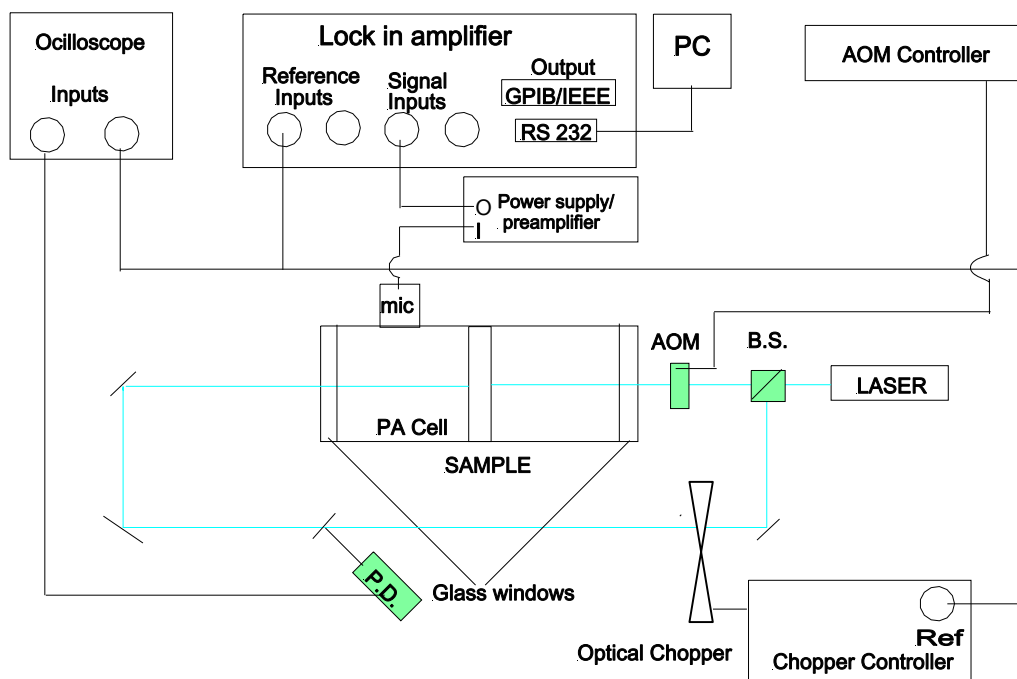


Figure 4.4 Schematic circuit diagram of thermal wave interferometer

When the sample is irradiated by the laser beams, acoustic signals are generated inside the cell, which are captured by the microphone detector and amplified by a preamplifier. This microphone detector is highly sensitive and prepolarised. It is connected to a power supply/preamplifier, through which signals are acquired. This signal is fed to the lock-in amplifier where it is further amplified, and then analysed and recorded by a PC. The reference signal from the optical chopper is connected to the lock-in amplifier to enable it to lock-in on particular signals and process them accordingly. The lock-in amplifier provides both amplitude and phase measurement for these signals. In double beam experiments, we measured the phase difference of the two resultant waveforms using the oscilloscope, however in single beam (one side excitation) we used the lock-in amplifier to measure the phase of the recorded signals.

A photograph of the thermal wave interferometer set-up is shown below mainly showing the cell assembly and some components.

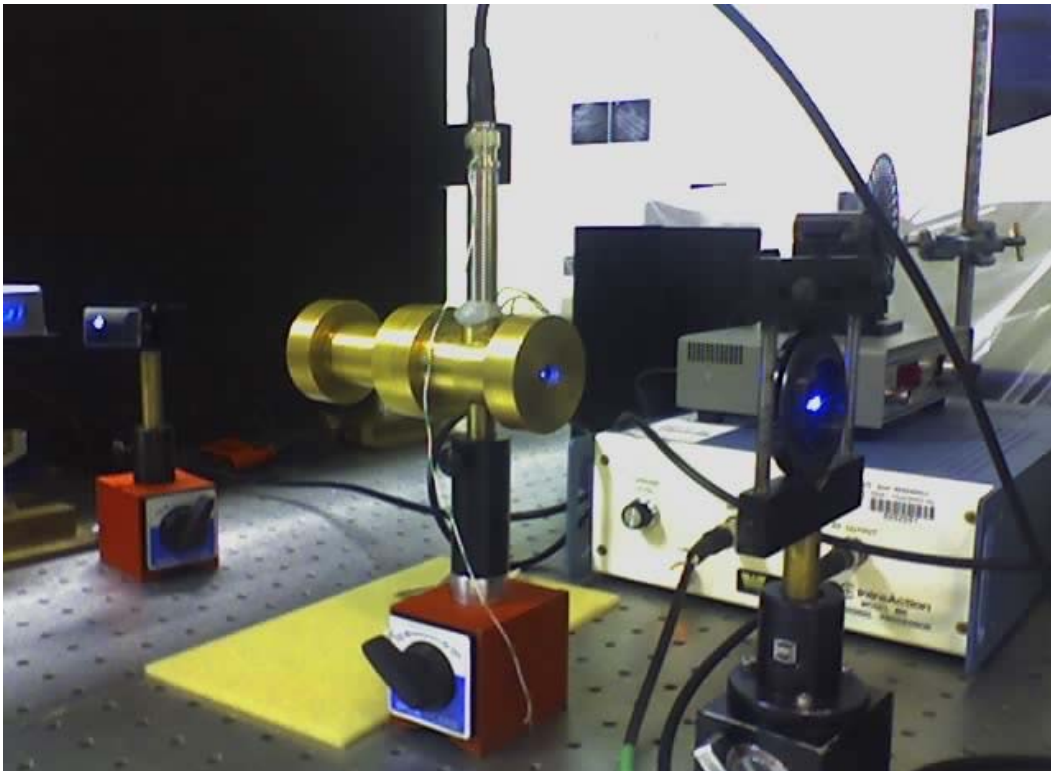


Figure 4.5 Picture of cell assembly in the experimental set up

4.4 Selecting the materials for testing

Before explaining the measurements further, it is to be emphasised here that how important the selection of material was for the samples and the theory behind it. To meet the requirement of thermal interference occurrence in a sample, a metal having larger diffusion length was needed. This is due to the highly damped nature of thermal waves. On working out the geometric length of most of the metals (elements) available on the basis of Equation (7) and using other characteristic data available from CRC handbook (1990-91) [34], it was found that for a given frequency calcium, copper and aluminium have the highest diffusion lengths in descending order.

The thermal diffusion length μ of a material, is defined in Chapter 3 by Equation (7), which is restated here,

$$\mu = \left(\frac{2\alpha}{\omega} \right)^{\frac{1}{2}}$$

where $\alpha = \frac{\kappa}{\rho c_p}$. For a modulated frequency of 10 Hz, the thermal diffusion length is

therefore given by $\mu = 0.178 \sqrt{\frac{K}{\rho c_p}}$. The values of the diffusion length are listed in Table

4.1 for the range of frequencies used in the experimental work reported in the next Chapter. Further, due to the unavailability of calcium in specific sizes and its non usability for all practical purposes copper and aluminium were chosen for the experiments.

Frequency (Hz)	Calcium (mm)	Copper (mm)	Aluminium (mm)
10	2.530	1.926	1.758
40	1.265	0.963	0.879
100	0.800	0.609	0.556
400	0.400	0.305	0.278
1000	0.253	0.193	0.176

Table 4.1 Thermal diffusion lengths

Hence all experiments were done on the samples prepared from pure Cu and Al metals. Samples of Cu and Al of diameter 14 mm and various thicknesses such as 100 μm , 500 μm , 1000 μm and 2000 μm were prepared and then polished. The samples were

coated with a fine carbon coating using a Dynavac coating unit (model CS-300) for heat absorption and to minimise reflections and scattering of the incident beam of light. In the final experiments uncoated samples were used to avoid any error due to carbon coating, although it was in the order of 1-2 μm only, which was verified by an optical microscope.

CHAPTER 5: MEASUREMENTS, RESULTS AND DISCUSSION FOR SINGLE BEAM EXPERIMENTS

5.1 Initial measurements of Photo Acoustic Signals (PAS)

Initially the sample was excited from the front side using only one beam from a He-Ne laser of maximum power 5 mW at 632.8 nm. On thermal interaction inside the cell, we could trace photo acoustic signals sensed by a highly sensitive microphone and then amplified by a preamplifier and recorded through a lock-in amplifier and oscilloscope. However it was almost impossible to record the signals at very low frequencies such as 10 Hz to 20 Hz. In Figure 5.1 different wave recordings are shown for 10 Hz, 14 Hz and 18 Hz. The graph shows the variation of the component $R\cos 2\phi$ from the lock-in amplifier, where R is the amplitude and ϕ is the phase angle of the waveform.

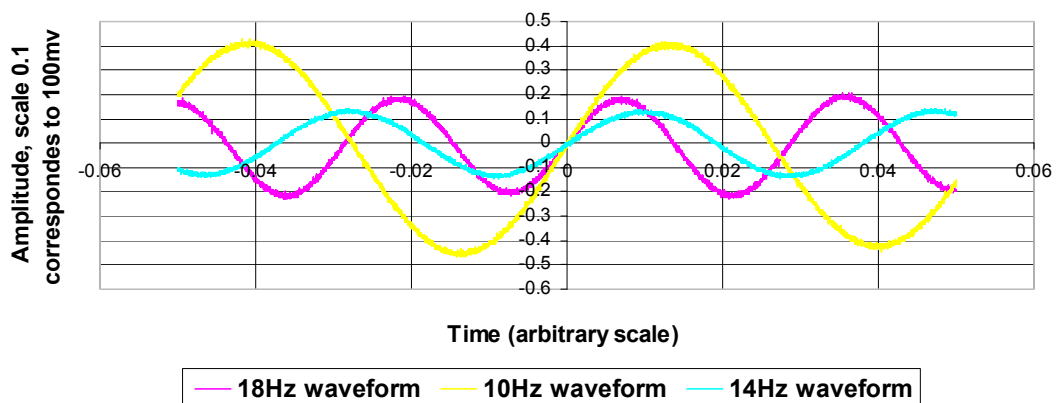


Figure 5.1 PAS amplitude waveforms at three different modulation frequencies for a 100 μm thick sample of Cu with 'front' excitation by He-Ne laser of power 1.98 mW at 633 nm

The signal to noise ratio was very high on such low frequencies, to overcome this problem we started using higher frequencies in subsequent experiments. We also replaced He-Ne lasers with a Class 3B air cooled Argon Ion laser emitting radiations of mixed wavelengths prominently the blue 488 nm of laser power up to approximately 100 mW, so that the same beam can be divided and the sample can be excited from both sides with the single laser. This avoided potential issues with instability in the power balance between the two lasers. A 50/50 beam splitter was used to split the beam in to two. One straight beam was incident

on front end of the cell, and the other beam orthogonal to it was steered by three plane mirrors to strike the sample from the rear end of the cell. Initially optical choppers were used in the path of both beams to modulate the beams. Using this arrangement a large number of scans were recorded for samples of copper and aluminium of different thicknesses. Although this technique helped in controlling the modulation frequencies, intensity and alignment of the beam, it did not resolve the problem of synchronization of the frequencies of two beams and measuring the phase difference ϕ between the two laser beams. However by using this arrangement valuable scans were recorded for either front or rear excitation for comparing data given by earlier researchers. Some are shown below in the following Sections. Further, it is to be remembered that phase measurements shown in Chapter 5 refer to the total phase lag ϕ_T , which may include the photothermal phase lag ϕ_{pt} , thermoacoustic phase lag ϕ_{ta} and thermal interference phase lag $\Delta\theta$.

5.2 Phase and amplitude analysis of Copper and Aluminium at different frequency ranges and its application in thermal interferometry

In Figures 5.2 and 5.3 we have shown the response curve of (thermal plus acoustic) phase lag and amplitude respectively with respect to the square root of modulation frequency for a copper sample of thickness 877 μm with thin (1-2 μm) carbon coating.

5.2.1 Copper results

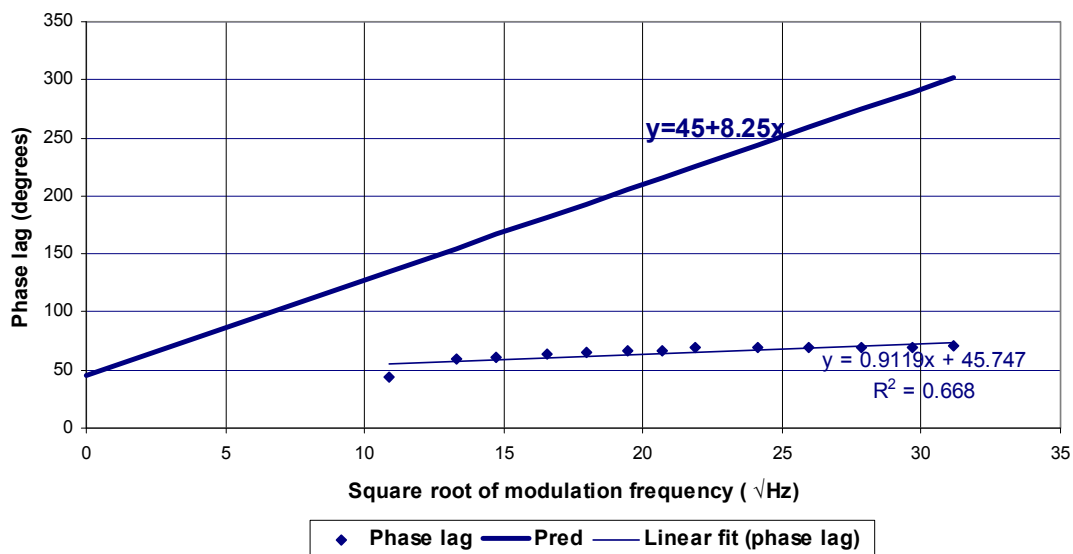


Figure 5.2 PAS phase lag for Cu, 877 μm thick, for front excitation

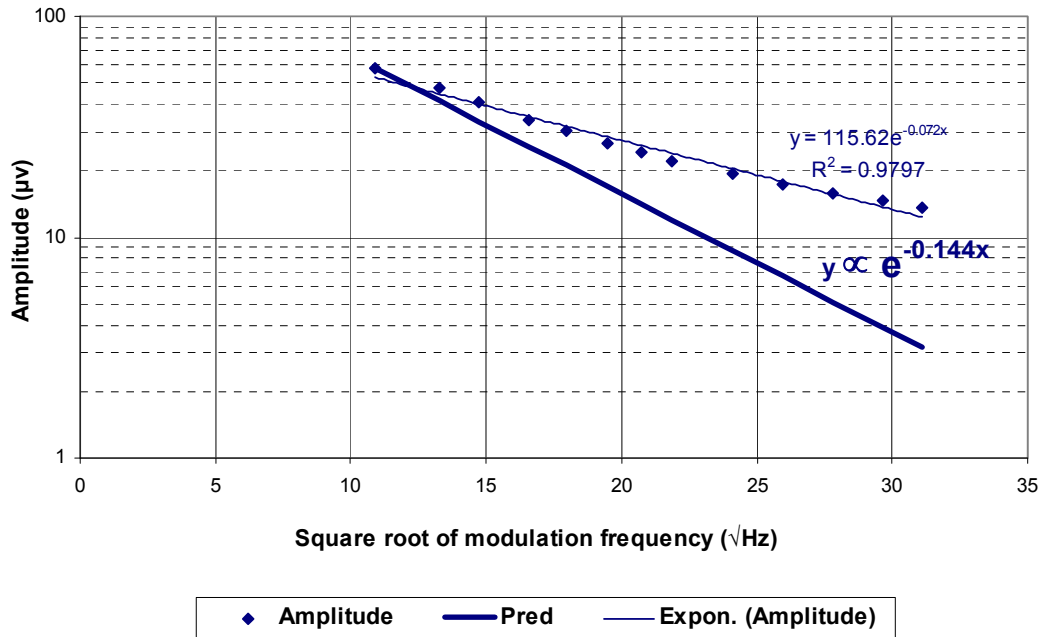


Figure 5.3 PAS amplitude for Cu, 877 µm thick, for front excitation

In Figures 5.2 and 5.3 the variation of phase lag and amplitude were recorded in the modulation frequency range of 100 Hz to 1000 Hz when irradiated from the front with an Argon laser beam of power 40.5 mW at mixed frequencies (mainly 488 nm).

In Figure 5.2 and 5.3 the value of y has been worked out using the formula for phase lag

$$\varphi_T = 45^\circ + \sqrt{\frac{\omega}{2\alpha}}L \quad \text{and for amplitude } A, \quad Ae^{i\varphi_T} \propto e^{(1+i)\sqrt{\frac{\omega}{2\alpha}}L}, \quad (41)$$

which should be valid as long as the sample thickness significantly exceeds the thermal diffusion length. According to Table 4.1, the 877 m copper can be regarded as thermally thick for this frequency range above 100 Hz. The results are consistent with the results obtained by earlier researchers [5], [6] and [8], however they differ from theoretical predictions, as the phase lag does not increase linearly and the amplitude does not decrease exponentially with increasing frequency as expected. However similar results have been obtained by other researchers in the past and it has been explained that the variation is due to additional phase lag predominantly due to thermal interference and in addition acoustic phase lag [5], [6], and [8]. It is to be noted that in both charts the slope (variation) is higher in the lower frequency range i.e. 100 Hz to 500 Hz (10-22 Hz^{1/2}). So

the changes in phase lag in this frequency range could be more useful in calculating thermal diffusivity.

5.2.2 Aluminium results

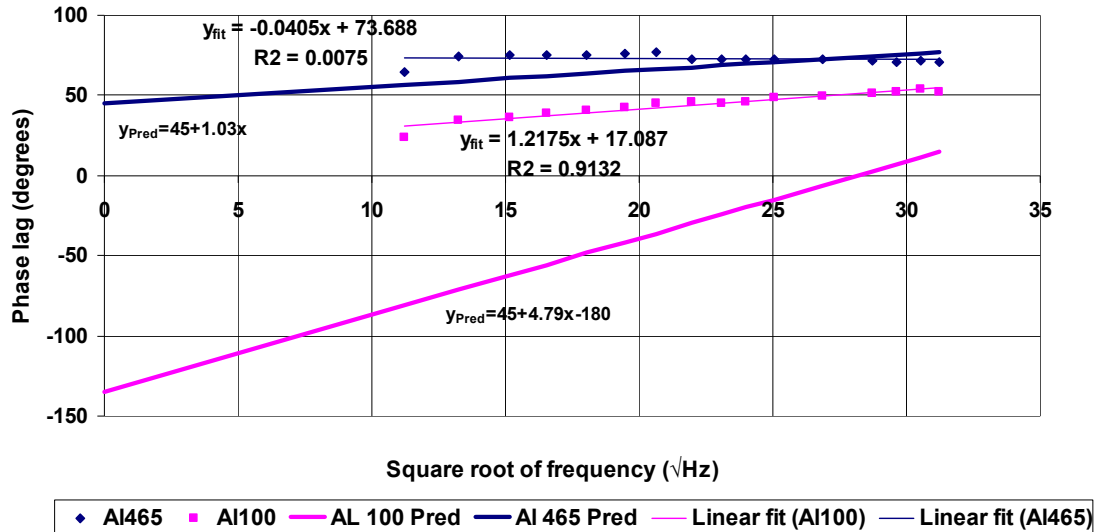


Figure 5.4 Phase lag for Al (Aluminium) samples of thickness 100 μm and 465 μm , for front excitation by Argon beam of power 18.2 mW

Figure 5.4 indicates that aluminium shows a higher value of phase lag in the 465 μm thick sample but remains almost constant in the higher frequency range. However in the Al sample of thickness 100 μm it is rising continuously indicating that the interference effects are prominent only in this sample. The results for copper will be introduced later in this Chapter.

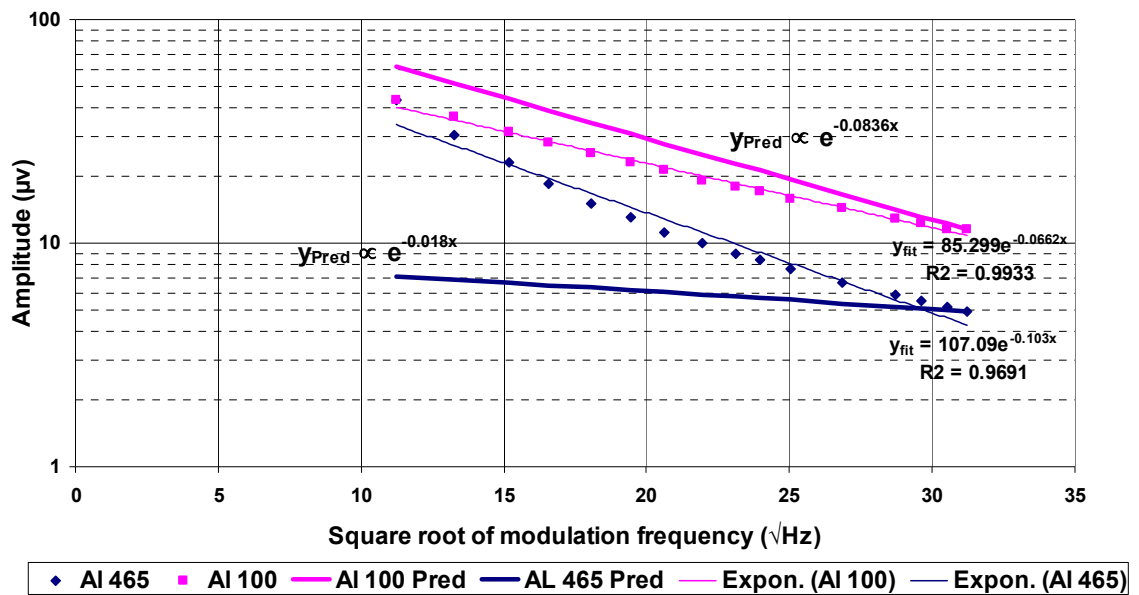


Figure 5.5 Showing variation of amplitude against frequency for Al samples of thickness 100 µm and 465 µm

In Figure 5.5 two graphs are shown for samples of aluminum of thickness 100 µm and 465 µm in which it is clearly noticeable that the amplitude value drops sharply towards higher frequencies similar to copper (also see Figure 5.3).

As the amplitude of PAS depends on many external factors other than the sample, such as laser power, the absorption, reflection and scattering of incident radiation, we concentrated only on phase measurement to achieve our goal.

5.2.3 Phase dependence on laser power

The fact that phase does not vary appreciably with respect to laser power is verified in the following result:

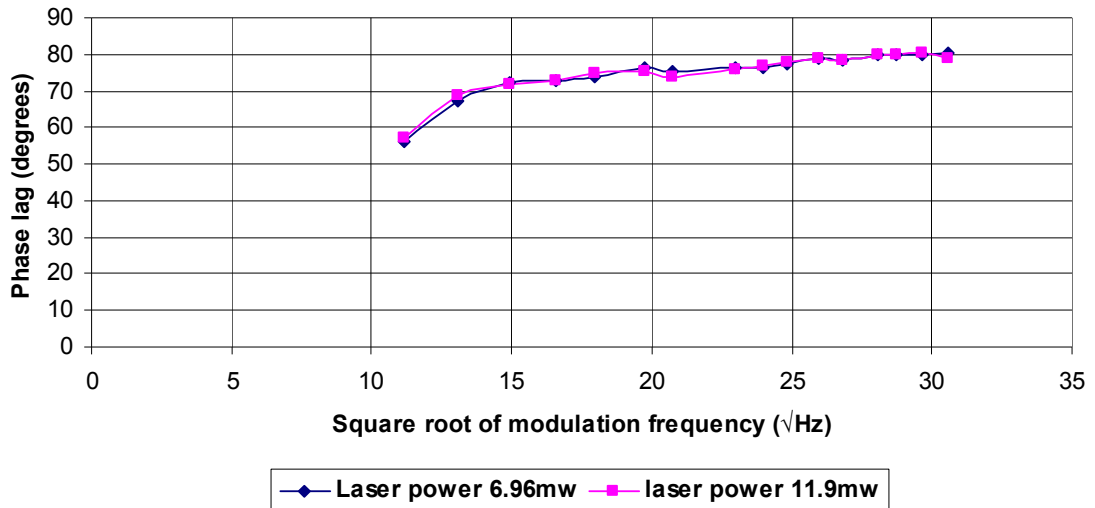


Figure 5.6 Comparison of phase lag response at different power levels of laser

Figure 5.6 shows the phase lag response of a Cu sample of thickness 950 μm with respect to the square root of modulation frequency at two different power levels of laser beam in front side excitation.

This graph shows that the response of phase lag is not affected by power of the laser beam, unlike amplitude. In this experiment, a Cu sample of thickness 950 μm was irradiated by Ar-Ion laser beams of power 6.96 mW and 11.9 mW for front side excitation and then the phase lag response was recorded over the same frequency range. It is evident that though laser power is almost doubled the response curves closely match each other.

Thermal interferometry has an important role in explaining the phase lag [5], [6], [8], [25] and [26]. The following measurements were done to further confirm the theories and extract useful information relating to this project.

5.2.4 Phase lag of Copper samples

The following scan is a comparison of the phase lag response of the two samples of the same material (copper) of different thicknesses measured under the same conditions.

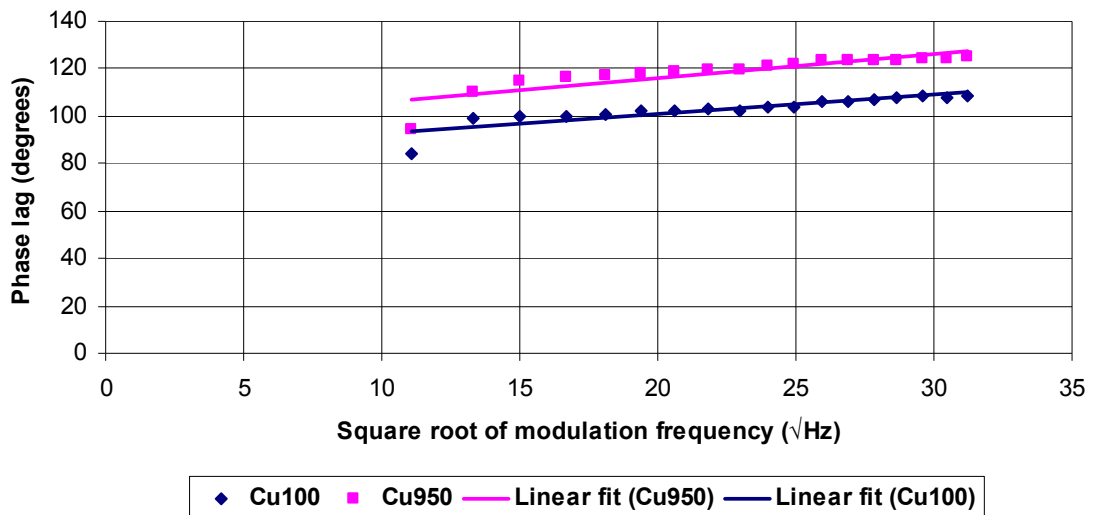


Figure 5.7 Phase lag for Cu of thickness 100 μm and 950 μm with glass backing and front excitation, Argon Ion laser power used 18.1 mW

When we tested two samples of copper with different thickness 100 μm and 950 μm , we found that the phase lag increases as a function of frequency but not linearly as expected, however the relative increase in the thicker sample (i.e. 950 μm) is much more than in the thinner sample (100 μm). This graph also shows that phase lag rises faster in the low frequency range compared to higher frequency range. For both the samples at the higher frequency range (500-1000 Hz or 22-32 $\sqrt{\text{Hz}}$) the curves are nearly flat. This is the reason that a very high frequency range is not suitable for our purpose of interference measurement.

In these scans glass backing was used behind the sample to support it. In the dual beam experiments in the next Chapter we removed it as the values obtained were affected by the reflection coefficient of glass and this was an error factor for further measurements in the dual beam experiments.

5.3 Phase and thickness relationship in copper samples

Experiments were done with copper samples of different thicknesses in front incidence and the relationship between phase lag and thickness of the samples was examined.

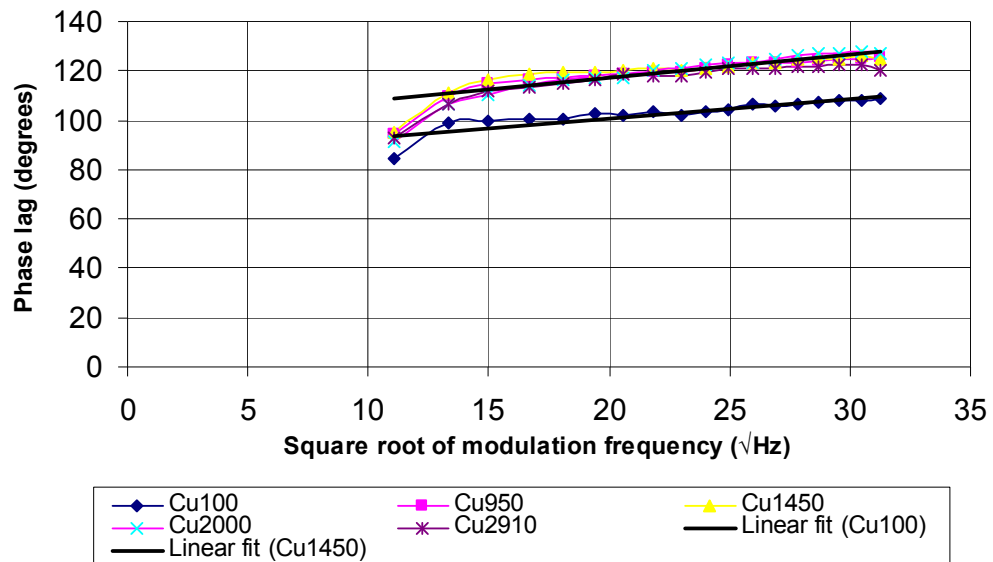


Figure 5.8 Phase lag for Cu samples of different thickness at different frequencies

Figure 5.8, shows graphs of five different sample thicknesses of copper irradiated on front side only in a single cell arrangement and explains that in all samples of Cu the phase lag increases with an increase in frequency and its values are higher in thicker samples compared to the thinner sample of 100 μm . However we do not find much difference in the values of phase lag relatively in samples thicker than 950 μm i.e. the relative phase lags for each sample 1450 μm , 2000 μm and 2950 μm are very similar. This is quite obvious as the curves for these three thicknesses are almost superimposed. This happens because when the actual thickness of the sample L exceeds μ , the thermal diffusion length, the interference effect tends to zero and hence there is negligible dependence of the phase lag on sample thickness. This is the reason that thermal interference effect is observed in thinner samples, where its effect is more significant.

This behaviour can be more easily explained by the following graphs for fixed frequencies and varying thickness of samples.

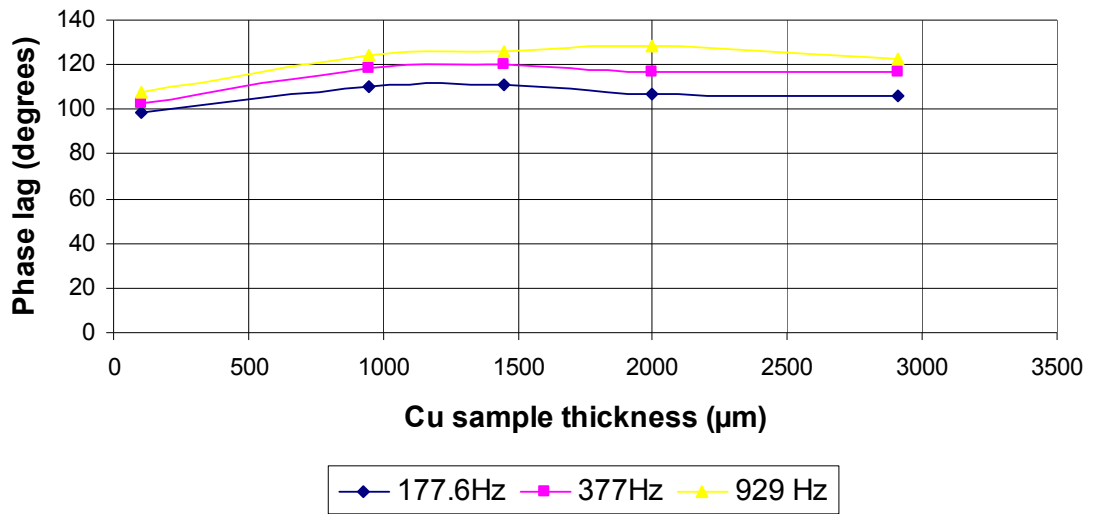


Figure 5.9 Phase lag variation against sample thickness for Cu at fixed frequency

In this Figure phase lag has been plotted against the varying thickness of copper sample for certain fixed frequencies in the range of 100 Hz to 1000 Hz. The curves show that there is an increase of phase lag with respect to sample thickness up to 1000 µm and after that it is almost uniform. Thus it is evident that these techniques (one side laser beam incidence in a single cell arrangement) are not useful for samples of thickness greater than 1 mm. The photo acoustic effects and interference of thermal waves can be observed only in thinner samples of a few microns (say 50-100 µm). Although these results are similar to the results obtained by earlier researchers, they are not very useful to conclusively explain thermal interference and hence can not be used to determine accurately the diffusivity of metals, or to measure coating thicknesses in applications like thermal barrier coatings, due to the uncertainty associated with all of the phase shifts contributing to the observed results.

5.4 Interpretation of single cell results

As we discussed and observed in this Chapter about the results obtained for copper and aluminium while measuring the phase lag and amplitude against the square root of the modulation frequency, we have found that although the results match and are qualitatively similar to those obtained earlier by other researchers [5], [6], [8] & [14], they do not follow the theoretical predictions fully. The variation of phase lag is not linear and amplitude values do not decrease exponentially with the square root of the chopped frequency as expected; it is believed that this discrepancy is due to many factors which have not been

accounted for, such as photo thermal response, absorption and reflection components of the incident beam, the thermal response from the walls of the cell, calibration of the detector microphone and acoustic phase lag. It is difficult to consistently predict and account for all of these factors simultaneously. But it is believed that the main contribution to the error is by acoustic waves, which would take some time to travel to the microphone and due to acoustic wave interference inside the cell. This discrepancy has been described by Jinan Cao [6], [8] and Almond and Patel [26] earlier as one of the main factors contributing to errors in measuring the phase lag of thermal waves by recording acoustic signals, as an acoustic phase lag is added due to the superposition of acoustic waves and their interference inside the cell. Other researchers have tried small enclosed cells and other types of single cells to minimise this effect, however to the best of our knowledge it has not improved the results considerably. The purpose of observing the thermal response in isolation has been defeated in the past due to this predominance of acoustic response in a single cell arrangement. In addition it is to be noted that in all these single cell experiments only one dimensional heat flow is assumed as the thickness of the sample is normally many times less than the width or diameter of the sample. Further, we believe that this aspect also has a bearing on the results and will be discussed further in Chapter 7.

To overcome the problem of acoustic phase lag, we developed a novel technique and used a double cell system, as described in the following Chapter. One could still argue that there would be an acoustic phase lag associated with this double cell arrangement as the microphone is situated in one of the cells. However, in the dual beam interferometer arrangement, one is only concerned with the relative phase delay between the two modulated beams for which a maximum or minimum acoustic signal is received by the microphone. The *acoustic* phase is no longer significant. In this way we not only eliminate the calibration requirement for the detector and cancel out instrument time constants, but we eliminate the acoustic phase lag as a factor as well. Hence we purely measure the thermal response. The photothermal response is also negligible as it is believed that the conversion of optical energy to thermal energy takes place in a period of less than 10^{-9} seconds [8] and the photothermal phase shift is the same on both sides of the sample.

Therefore the biggest advantage of this technique is that acoustic phase lag is completely eradicated and thus it can be used to achieve and explore further applications where accuracy of the thermal response measurement is vital.

CHAPTER 6: MEASUREMENTS, RESULTS AND DISCUSSION FOR DUAL BEAM EXPERIMENTS

6.1 Thermal interferometer set up achieving null effect

We used the design of the laboratory thermal interferometer shown earlier in Chapter 4 (Figures 4.3 and 4.4) for the dual beam experiments. In this set up the samples were irradiated from opposite glass windows of the double photo acoustic cell and acoustic signals were recorded by a microphone mounted perpendicular to the side wall in one of the cells. The samples had no coating and were finely polished. As described earlier a single high power laser beam was split into two beams using a beam splitter and using a few plain mirrors the beams were steered to the cell from two opposite directions and were made incident on the centre of the sample. The microphone recorded the acoustic waves generated after the interaction of thermal waves inside the sample.

The laser power on each face of the sample was adjusted to achieve a 'null effect', where the amplitude of the acoustic signal was approximately zero due to the thermal waves meeting in nearly opposite phase at a certain phase difference between the two laser beams. In order to observe the phase shift ϕ of one beam with respect to the other we used an innovative technique. In this technique we mounted an optical chopper on a mini translation stage on the optical table, and on moving the chopper blade on this stage in the path of the beam we could get the desired phase shift of one beam with respect to the modulation introduced on the other beam by the acousto-optic modulator. The recordings were done by moving the chopper blade slowly using the translation stage to read zero amplitude on the lock-in amplifier. A large number of scans were recorded by moving the optical chopper for the entire width of opening of the chopper blade to cover the maximum phase difference introduced between the two beams. These scans covered mostly a range of phase shift ϕ of over 0-180° with a minimum and maximum for the acoustic signal amplitude recorded at each of the phase shifts. We did this for different samples and at different levels of laser power as required to excite the samples adequately. These results are discussed in this Chapter.

Although there was a limitation in the scan range (which was maximised by adjusting the height and position of the blade) the range was sufficient for our purposes. Figure 6.1

shows the mechanism of the phase shift introduced by the chopper.

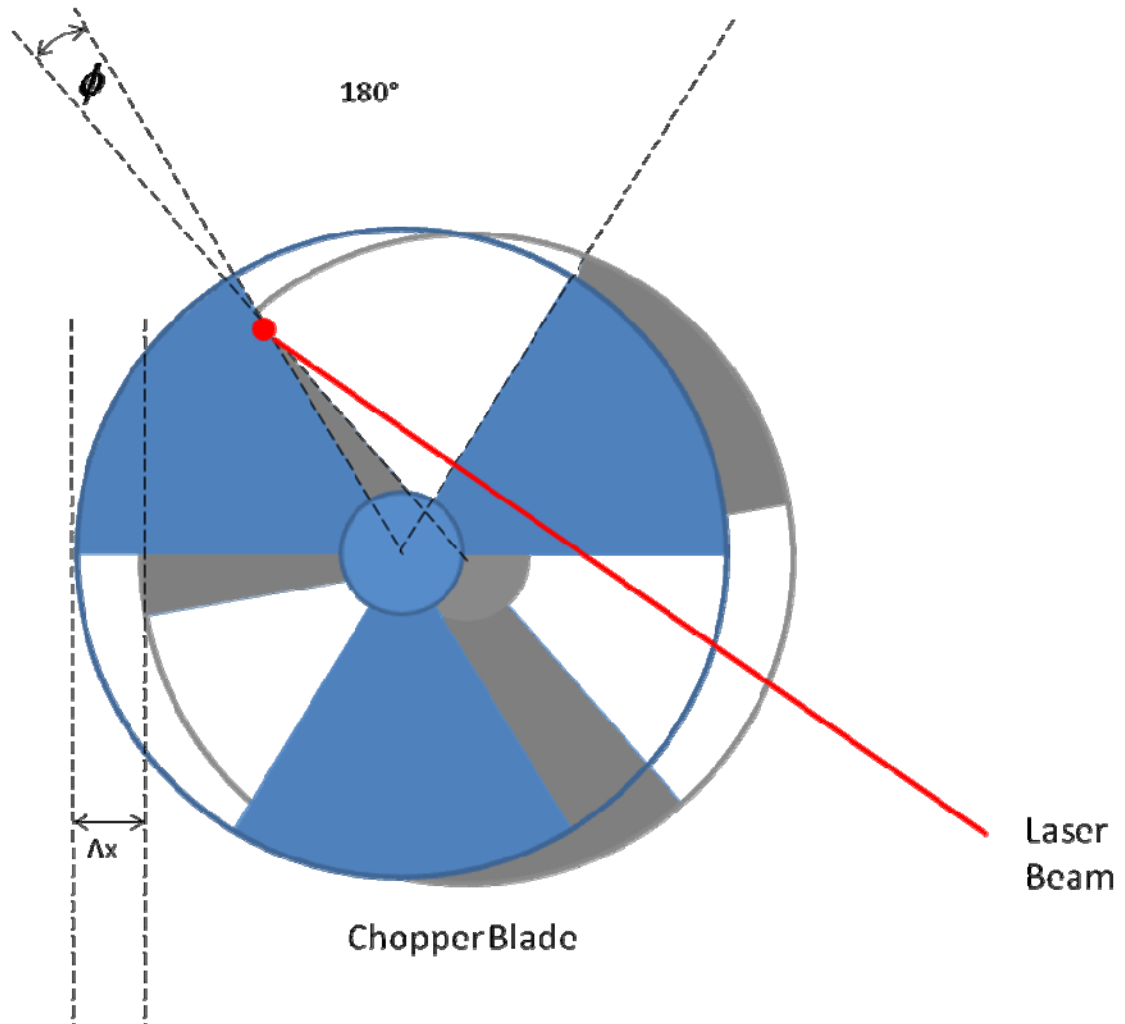


Figure 6.1 Diagram showing phase shift mechanism

In Figure 6.1 for convenience only a 3 slot chopper blade is shown, however in practice a 6 slot chopper blade was generally used.

In this mechanism the optical chopper blade cutting one of the laser beams perpendicularly is moved horizontally while keeping the beam fixed, so that a phase difference (or phase shift) ϕ is created in the beam with respect to the beam modulated by the chopper reference signal at the AOM. Whatever the phase shift, the chopping frequency remains the same for both beams and this synchronisation is maintained

through the chopper reference signal. Thus at a synchronised modulation frequency the amplitude of acoustic signals generated are measured for varying phase shift of the two incident beams. In this process maximum and minimum values of acoustic amplitude are recorded and can be compared to theory.

Figure 6.2 was recorded for a copper sample of 100 μm at a modulation frequency of 126.5 Hz. The phase difference between the waveforms of two laser beams was recorded using the oscilloscope. The synchronization of the modulation frequency for both the beams was also verified by the oscilloscope. Minimum amplitude resulting in a zero or near zero value (0.01 - 0.02 μV) was achieved by adjusting the chopper blade position, as already described. The phase shift measured for the equilibrium condition (achieving 'null effect'), is also referred to as the 'null phase difference' in the following discussion. This technique was used to record several scans for samples of different thickness.

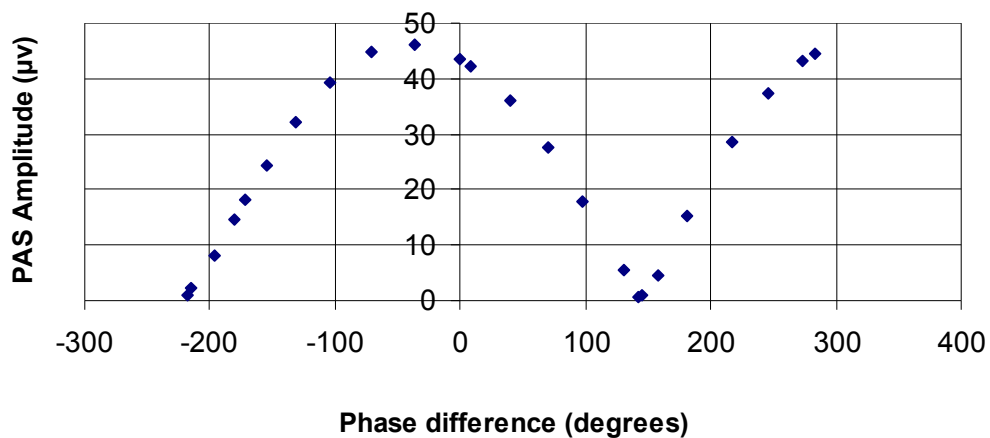


Figure 6.2 Interference curve for Cu, 100 μm thick at 126.5 Hz

The similar graphs recorded for copper samples of 160 μm , 250 μm and 500 μm on a fixed modulation frequency of 126.5 Hz, are shown in Figures 6.3, 6.4 and 6.5.

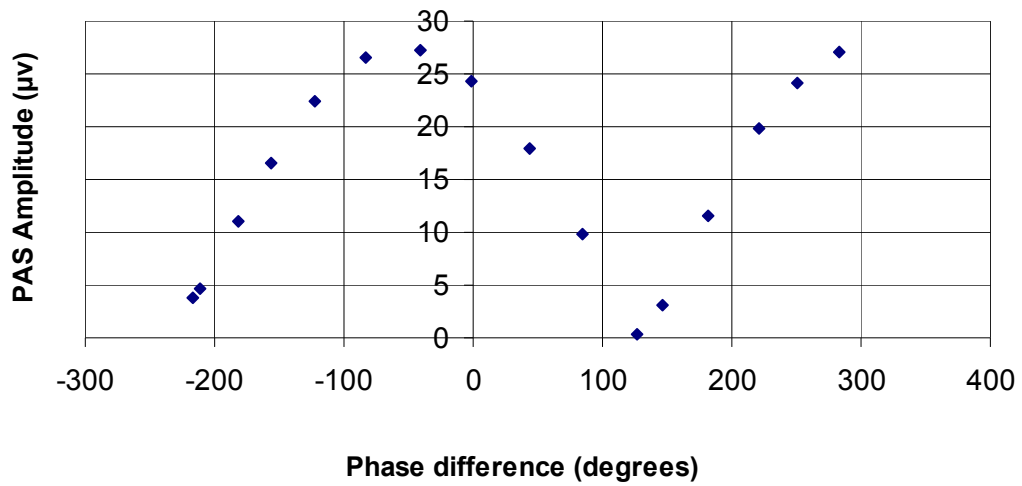


Figure 6.3 Interference curve for Cu, 160 μm thick at 126.5 Hz

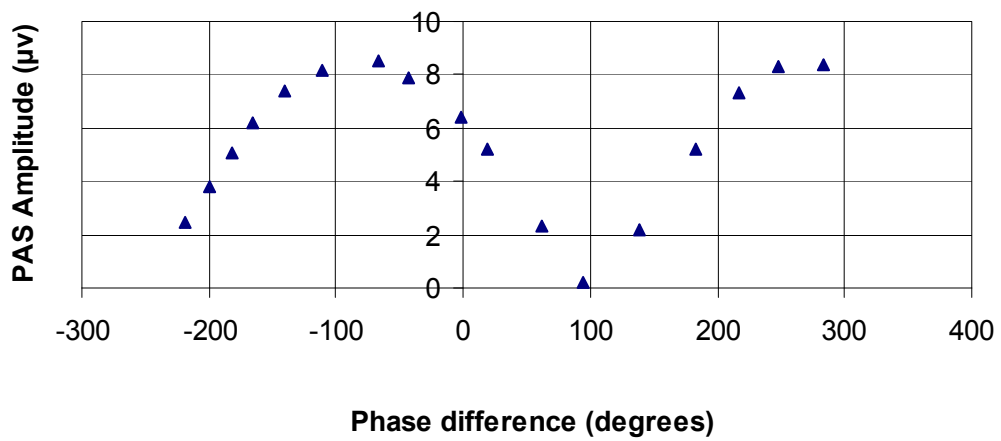


Figure 6.4 Interference curve for Cu, 250 μm thick at 126.5 Hz

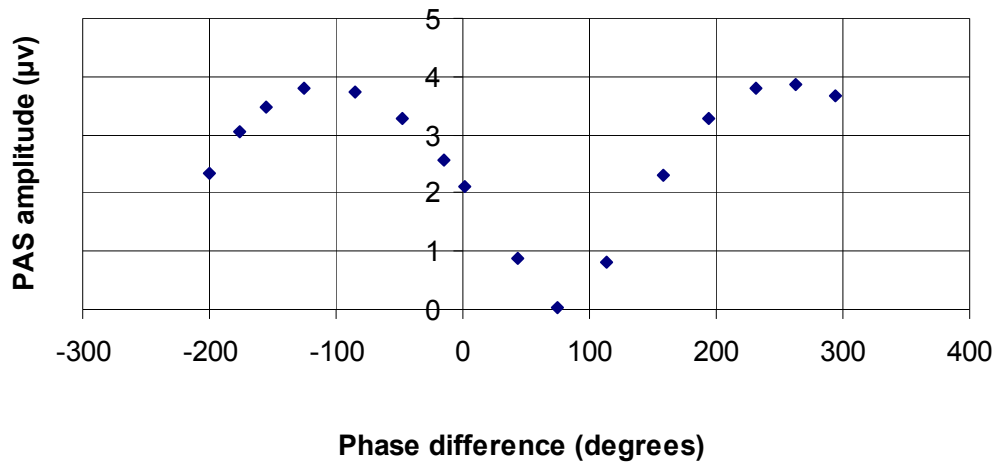


Figure 6.5 Interference curve for Cu, 500 μm thick at 126.5 Hz

One can easily observe the change in phase dependence when sample thickness is changed. The null phase shift decreases with increasing sample thickness. The data is analysed in Chapter 7.

6.2 Accuracy and variance in recorded results

In Figure 6.6, we compare values recorded for copper sample of thickness 100 μm for two scans recorded at different times at the same frequency of 126.5 Hz to show the variance in results due to limitations in the experimental set up.

6.2.1 Accuracy

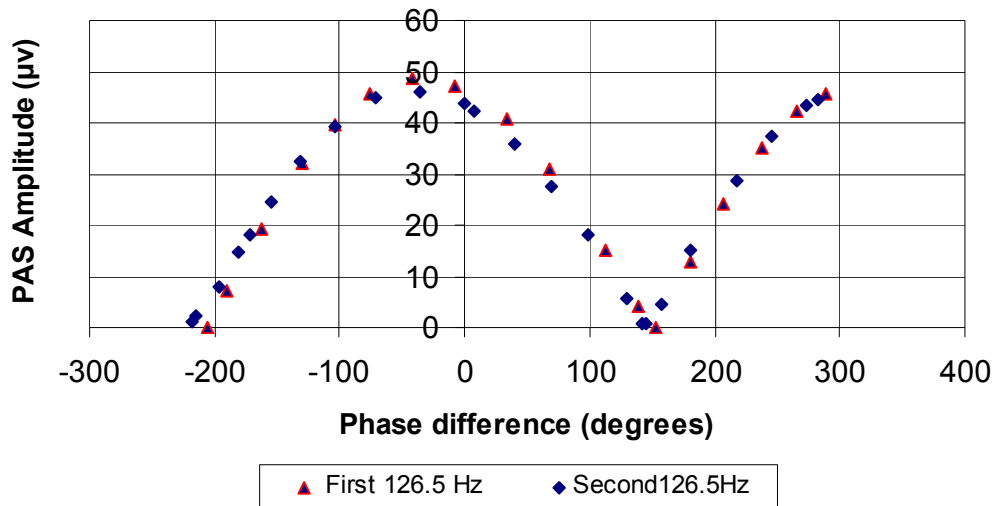


Figure 6.6 Two interference curves for Cu, 100 µm thick at 126.5 Hz

At two different times of measurement the difference between the response curves is small. It is to be noted that these scans were taken at an interval of a couple of months and during that period samples were changed many times and other adjustments were also done. Further scans reinforced this finding.

6.2.2 Variance

We recorded some more scans using two different samples of Cu obtained from different sources, but of the same thickness. Graphs were plotted for the two different samples and are shown in Figure 6.7.

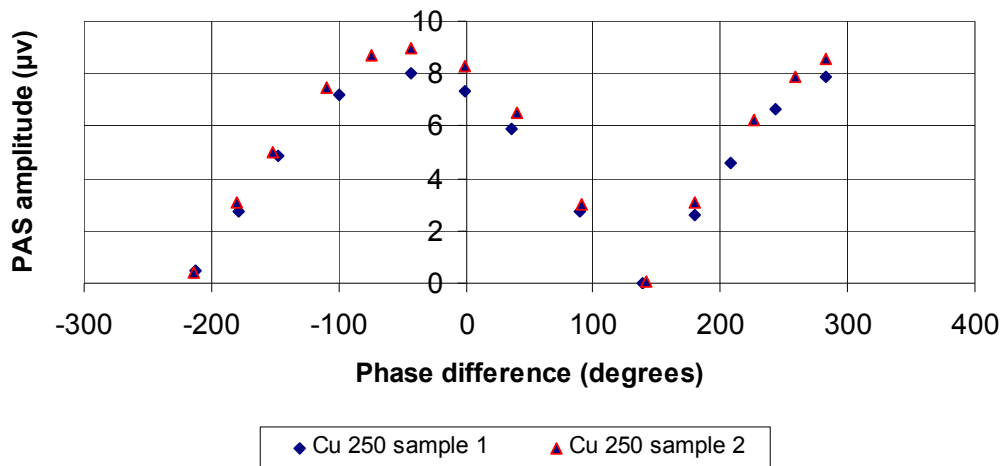


Figure 6.7 Interference curves for samples of Cu, 250 μm thick, from two different sources

There is some variance in the maxima, which is due to the varying thermal response from the two different samples and it could be due to a number of reasons; however at the null point they are close together which is to be expected as both the samples are of copper and of the same thickness. One sample was cut from a copper rod as a slice of thickness 250 μm , however the other was cut from a copper sheet of 250 μm thickness and they were procured from different suppliers. But the copper sheet surface appeared different to the sliced piece of copper from the rod. Although both samples were polished finely and prepared to the same geometrical dimensions, but there is a possibility of variance in their characteristics due to minor changes in purity or other reasons. It further implies that a more correct analysis is possible by measuring the phase lag in the thermal response instead of the amplitude, as the amplitude can vary for different reasons.

6.3 Power data analysis

$$A_{100} = 0.0292e^{0.0449x}$$

$$R^2 = 0.973$$

$$A_{500} = 0.0014e^{0.0618x}$$

$$R^2 = 0.9866$$

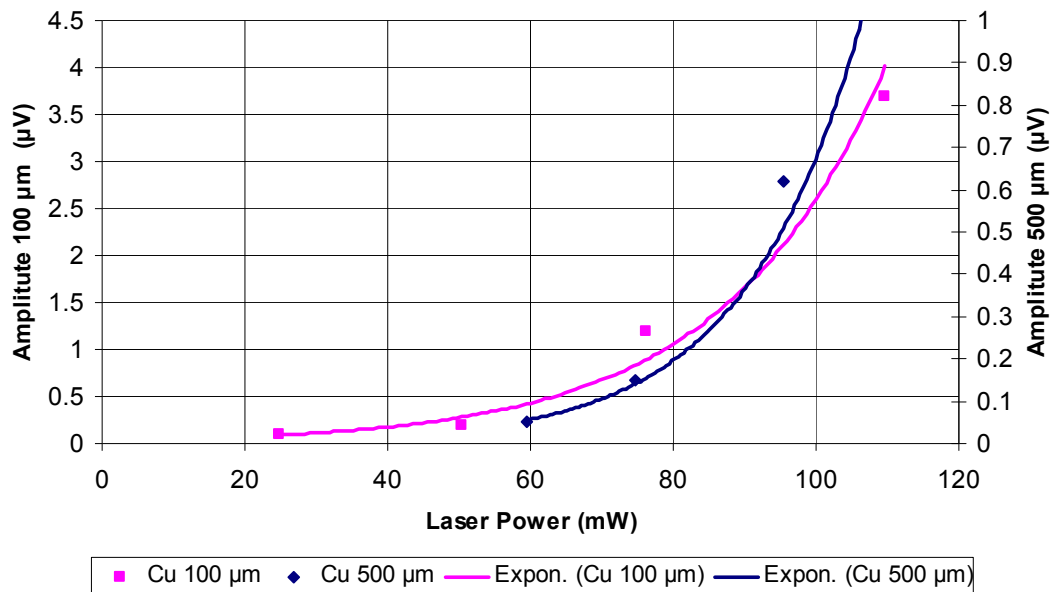


Figure 6.8 Minimum amplitude versus laser power

Using the double cell system set up, we measured the minimum amplitude for varying power of the laser beam, which is shown in Figure 6.8.

Both measurements seem to show an exponential dependence on the amplitude as the data provides a reasonable fit to the expression $A = A_0 \exp(P_{mW}/20) + A_{noise}$. However, the null phase difference remained fixed within “noise” levels indicating that the phase lag is independent of laser power. Fortunately it is only the phase difference that is important in working out the thermal diffusivity of the sample.

The minimum amplitude of the measured sound apparently increases exponentially with the laser power; however the relationship should be linear as amplitude is directly proportional to the laser power, according to Equation (15). This can perhaps be explained in terms of a convection cell that is setup within the device, which cools the sample more

strongly as the mean temperature of the sample rises. The convection cell will give rise to a boundary layer next to the sample surface and the thickness of the natural convection boundary layer depends inversely on the laser power raised to some power (index) or an exponential function of the laser power. Thinner boundary layers result in better coupling of the temperature fluctuations on the sample surface to the sound levels produced in the cell. This might explain the unexpected dependence of sound amplitude on laser power.

There is also a possibility that the laser beams become more unbalanced at higher total power and this imbalance creates a higher power differential.

CHAPTER 7: ANALYSIS OF THERMAL INTERFERENCE RESULTS IN DETERMINATION OF THERMAL DIFFUSIVITY

7.1 Thickness versus phase difference (shift) results

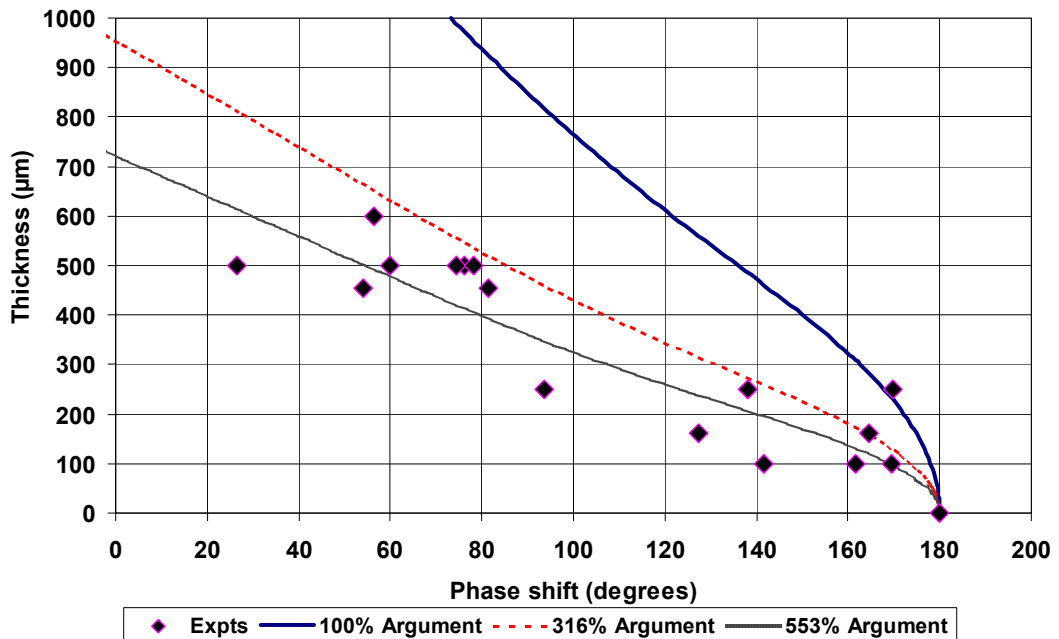


Figure 7.1 Comparison of sample thicknesses versus null phase shift at 126.5 Hz

In this Chapter the relationship between phase shift and thermal diffusivity is examined in more detail. Figure 7.1 is plotted using a set of results recorded using the thermal interferometer set up for different samples as described earlier. The expression developed in Chapter 3 (Equations 37 and 38) was used to predict the phase required for maximum and minimum signals from the experiment.

The experimental data may be compared with the theory, using the thermal diffusivity value of copper as $\alpha = 1.16 \times 10^{-4} \text{ m}^2 \text{ s}^{-1}$. Three theoretical curves are plotted using Equation (37) with different values of the *Argument*, where $Argument = \gamma L = \sqrt{\frac{\omega}{2\alpha}} L$.

The predicted curve shown by the red line (316% *Argument*) differs from the standard value for the thermal diffusivity of pure copper, given by the solid blue line showing the 100% *Argument*. The best agreement with the data is given by the curve calculated with 553%

Argument, or 5.53 times the expected value of the *Argument* based on the published value for the thermal diffusivity of copper.

In attempting to explain this significant discrepancy, it is to be noted that all of this data was recorded at a relatively low frequency of 126.5 Hz, at which the signal to noise ratio is relatively high and signal output is not very stable. Although this may account for some of the scatter in the data, it does not appear to account for the significant systematic shift relative to the expected value. The purity of the copper samples was not accurately specified by the suppliers and was expected in the range of 98-99%. It is not expected that this level of impurity would account for the large deviation observed in Figure 7.1. We will discuss some other possible reasons for these variations as follows:

7. 1.1 Interpretations

a) Path length

One possibility is that the setup “sees” a longer thermal path length than just the thickness of the sample. This could be interpreted as due to misalignment of the laser beams. The correction factor (parameter multiplying the argument) required to get agreement being the actual distance between the two beams centres divided by the sample thickness. This might explain the large amount of scatter exhibited by the fixed frequency data. Every time the sample is changed, the alignment is slightly different. In contrast, the setup and therefore the alignment is more stable for data taken from a single sample of fixed thickness. However repeat measurements with a more precise alignment did not deliver an appreciable improvement in the results.

b) Varying phase changes at the surfaces

There is also the possibility that the boundary conditions at the surface of the sample are somehow changed or varying. The theory predicts that a 45° phase change occurs when the heat flux on the surface produces a temperature field. However there are heat losses from the surface, so this is not quite true; after all the sound is generated from surface heat losses. However to explain some of the extra phase needed to explain the variable thickness experiment, phase lags of over 100° are needed. So this also seems unlikely.

7.2 Further analysis of data and its interpretations

In order to better understand the discrepancy observed in Figure 7.1, measurements were made of the phase shift ϕ required to obtain a signal minimum for a single sample of 100 μm thick copper shim. The frequency was varied from 170 Hz to 1232 Hz. The expression developed in Chapter 3 (Equations 37 and 38) was used to predict the phase required for maximum and minimum signals from the experiment.

The experimental data may be compared with the theory, again using the $Argument = \gamma L = \sqrt{\frac{\omega}{2\alpha}} L$ as defined before, with the thermal diffusivity value of copper $\alpha = 1.16 \times 10^{-4} \text{ m}^2 \text{ s}^{-1}$. The results are shown in Figure 7.2, with the two sets of experiment; one used a six slot chopper blade, the other a 30 slot chopper blade, to generate the frequencies. The theory is plotted using Equation (37) multiplied by factors of 1, 1.3 and 1.7.

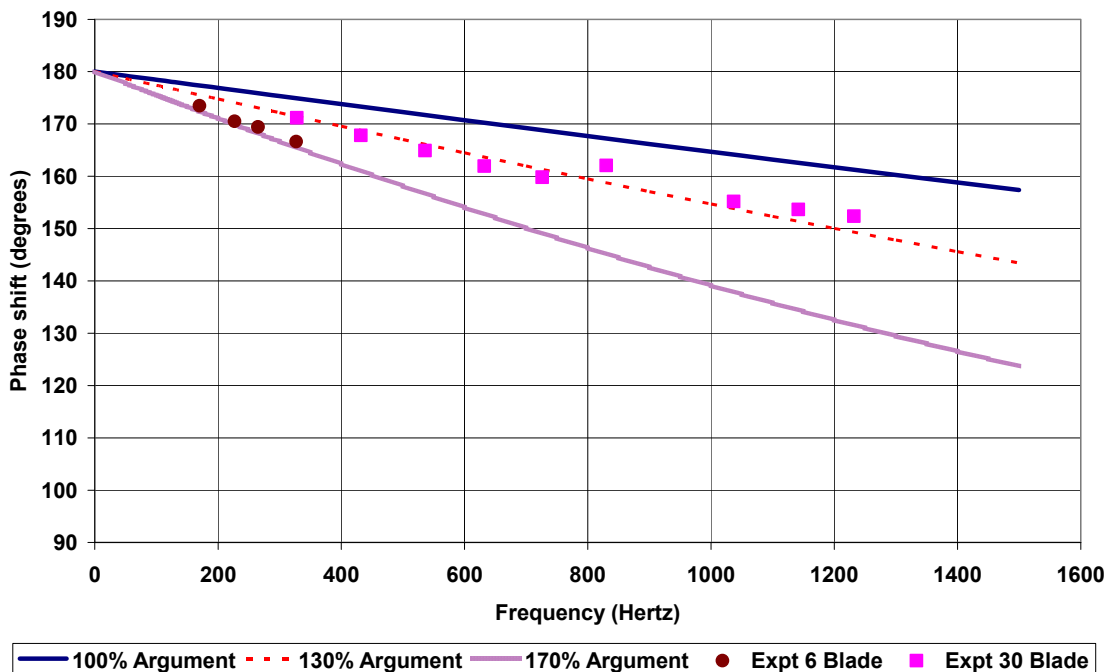


Figure 7.2 Null phase shift versus frequency for Cu, 100 μm thick

In Figure 7.2 it can be seen that the low frequency (six slot chopper) results fit well with the theoretical prediction with the argument multiplied by 1.7, and the higher frequency data (30 slot chopper) fits best when the argument is multiplied by 1.3.

In comparison with the results of Figure 7.1, we can see that the results in Figure 7.2 are in much better agreement with the theoretical predictions. It is to be noted that the best agreement is in the modulation frequency range of 300 Hz to 1300 Hz in Figure 7.2, while the data recorded in Figure 7.1 was at a fixed modulation frequency of 126.5 Hz. In the following Section 7.3, we have tried to explain other possible reasons contributing to errors in the results recorded during these experiments.

7.3 Effect of spot size on thermal interference experiments

The effect of laser spot size on the phase lag observed in thermal wave interferometry experiments has been analysed in full by Fabbri and Cernuschi [35]. This analysis shows that for smaller laser spot sizes the approximation of 1D heat propagation breaks down and the 3D heat flow leads to phase deformation. The full analysis is complex and beyond the scope of this thesis.

A simple argument is presented here to estimate the effect of spot size on the phase lags measured in the thermal wave interference experiments. The spot size in our experiments is estimated as 4 mm and the sample diameter = 14 mm.

The laser spot will have a 1D phase lag and an additional phase lag from an “edge effect”, similar to the calculation of the capacitance of two discs. Looking from the top in Figure 7.3 the laser heated region is in red and the “edge effect” region is in pink.

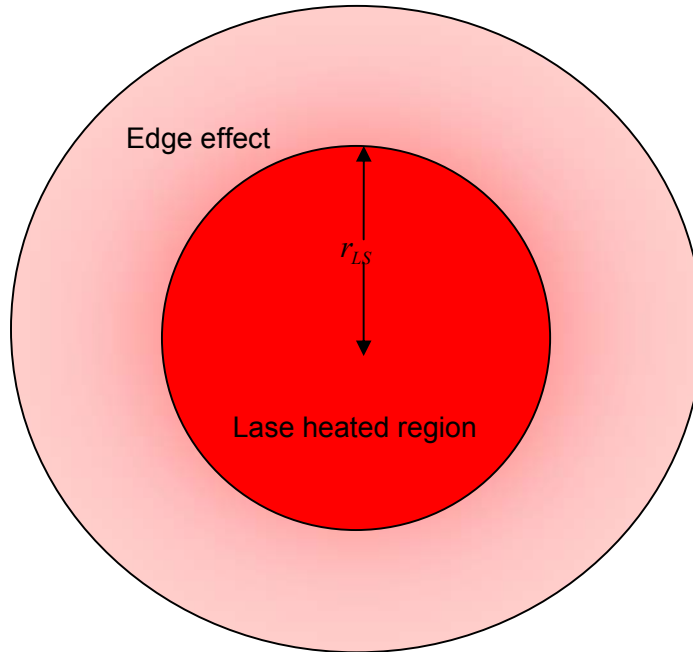


Figure 7.3 Diagram of edge effect due to finite laser spot size

The laser heated region has an area:

$$A_{LaserSpot} = \pi r_{LS}^2 \quad (42)$$

Where r_{LS} is the diameter of the laser spot. This contributes a phase lag of ϕ , which for convenience will be taken as zero in the absence of an edge region. In other words the phase lag caused by the laser spot region will be taken as the standard.

The edge region will have width beyond the laser spot of about μ , the thermal diffusion length (given by Equation 7). Thus the area of the edge region is given by:

$$A_{Edge} = \pi(r_{LS} + \mu)^2 - \pi r_{LS}^2 \quad (43)$$

and will be assumed to contribute a phase lag $\phi + \theta$ on average. That is an additional phase lag of θ .

The two areas will contribute to the overall measured phase lag, by interference between the two signals from each area, thus:

$$S = A_{LaserSpot} \sin(\phi) + A_{Edge} \sin(\phi + \theta). \quad (44)$$

The condition for a minimum to occur (both areas to destructively interfere) is:

$$S = 0 = A_{LaserSpot} \sin(\phi) + A_{Edge} \sin(\phi + \theta) . \quad (45)$$

This gives a phase lag ϕ of zero, if there is no contribution from the edge effect. This is the expected correction for no edge effect. This condition yields the relationship between the additional phase shift and the new phase shift corrected relative to the phase shift expected without the edge effect:

$$\tan(\phi) = -\frac{\beta \sin(\theta)}{1 + \beta \cos(\theta)} , \quad (46)$$

where:

$$\beta = \frac{A_{Edge}}{A_{LaserSpot}} = \frac{(r_{LS} + \mu)^2 - r_{LS}^2}{r_{LS}^2} = \left(\frac{\mu^2}{r_{LS}^2} + \frac{2\mu}{r_{LS}} \right) = \left(\frac{2\alpha}{\omega r_{LS}^2} + \frac{2}{r_{LS}} \sqrt{\frac{2\mu}{\omega}} \right) . \quad (47)$$

Below is a plot of the “edge effect” correction for a 4 mm diameter laser spot shining on aluminium and copper samples. The average phase shift due to the edge effect alone θ is assumed to be 90°.

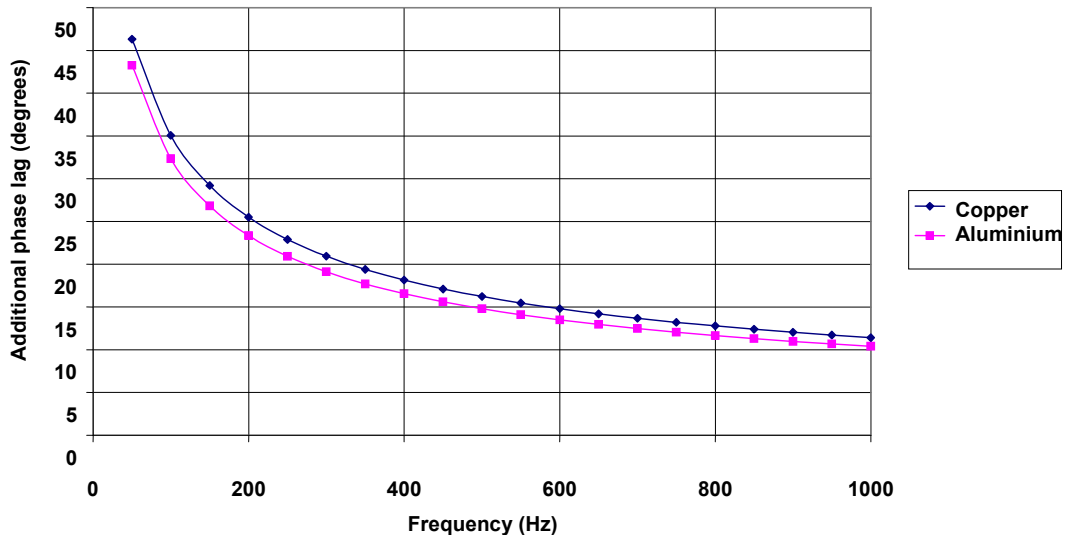


Figure 7.4 Additional phase lag plotted against modulation frequency for Cu and Al for a 4 mm diameter laser spot with $\theta = 90^\circ$

At 125 Hz the expected additional phase lag is 32° for copper and 29° for aluminium, which is comparable in magnitude to the errors of approximately 30° observed in case of a sample of thickness 200 μm in Figure 7.1.

This is a rough analysis and should only be taken as an estimate in place of a full 3D analysis. However, this analysis suggests that finite laser beam size effects can lead to a phase deformation that is comparable in magnitude to the discrepancy observed in the results of Figures 7.1 and 7.2. In general, the 1D approximation is only valid when the thermal wavelength $\lambda_{th} = 2\pi\mu$ in the sample is much smaller than the laser spot size [35]. Consequently by the definition of the thermal diffusion length in Equation (7), the 1D approximation can be expected to be less accurate at low frequencies.

CHAPTER 8: CONCLUSION AND RECOMMENDATIONS

In this research work a considerable success has been achieved in showing physical evidence of thermal wave interference' and a "thermal interferometer" has been used to explore the characteristics of photo acoustic signals. The phase and amplitude of acoustic signals from copper and aluminium were recorded for various samples and analysed accordingly. This research work highlighted the use of a double cell system, which has a distinct advantage over a single cell system in measuring the thermal response of thin samples of metal. This technique was also helpful in demonstrating thermal interference by the "null effect" approach and could be used for the determination of thermal diffusivity of the materials.

It is evident from the experiments and results that this thermal Interferometer set up is highly sensitive and there are many constraints which affect the results. Initially it was noticed that environmental noise such as building vibration, interference of electric fields and noise from an air conditioner were some of the main reasons for variance in the recorded acousto-optic signals. These were overcome by using a vibration isolation optical table and other standard isolation techniques. Other technical difficulties were noticed at later stages of the experiments and they were addressed accordingly such as alignment of the laser beam, coating of the samples and instrumental limitations.

We also introduced a technique of moving the optical chopper in the path of one beam to create a phase shift with respect to the other. We utilised an oscilloscope to measure the shift in waveforms relative to frequency and also observed the null effect by observing signal amplitude values from the lock-in amplifier. However it was hard to determine the exact position of the stage for a maximum or minimum as the shapes of the square waves were not exactly square and it created an error of at least 2 to 4 degrees while reading the phase shift. This error also accounts for the variation of data due to a noise in the lock-in amplifier. Also the change of chopper blades creates some problem as slight variation in the angle of the blades to the incident beam results in varying frequency of up to 1 Hz. At the same time the purity of material supplied was also unknown. So there were a number of reasons contributing to the variation in the values recorded.

Here we would like to describe an important aspect of the experiment, which might be a

major factor in contributing to the results in this thesis and that is, the assumption of 1D heat flow. Earlier researchers also have the same consideration of heat flow in one dimension only. It is very obvious that heat will flow in all directions in the sample as heat has a tendency to diffuse in a medium. This aspect has been ignored by most of the researchers on the grounds that the thermal thickness of the sample is many folds less than the width or diameter of the sample and the diameter of the laser spot. Although it is certainly known that the assumption of 1D heat propagation breaks down when the thermal wavelength is comparable to the laser spot size [35], the full theoretical explanation of 3D flow of heat energy is beyond the scope of this thesis; however we have tried to explain its 1D effect by a simplified analysis of the effect of spot size on thermal wave interference in Chapter 7.

Most of the problems have been addressed to an extent; however the most important was introducing a phase shift on synchronized frequency of both the beams by moving the chopper blade. The manual process of moving the chopper blade on one of the beams was found to be an imprecise method and contributed to errors. This problem can be overcome by using an electronic shifter. This could not be achieved within the scope of the project, but would be worth addressing in future work.

This study and project outcome reveals that the measurement of thermal interference is possible and projects a vision for a commercial thermal interferometer in future. Further, this thesis contributes mainly by the innovative development of a novel technique of phase analysis using the “null effect” for photo acoustic studies. This technique also highlights the advantages of using a double cell system with dual optical irradiation over a single cell and single beam system for the study of thermal wave interference. It also shows that a full three dimensional analysis will be required unless the spot size can be made much larger than the thermal thickness of the sample. Effectively the laser beam should cover the entire sample; however expanding the beam to cover the entire sample creates further limitations in recording the results. The desired level of laser intensity is drastically reduced and hence the advantage of using a laser to obtain rich signals even with the moderately thicker samples (100-1000 μm) is compromised and the signal to noise ratio may degrade.

We foresee a large potential for further research on this topic and expect a commercial model can be developed in the future, which can be used for research and other industrial applications.

REFERENCES

1. A.G. Bell, Am. J. Sci. 20, 305 (1880)
2. A. Rosencwaig and A. Gersho, J. App. Phys. 47, No.1, (1976)
3. J. Tyndall, Proc. R. Soc. London 31, 307 (1881)
4. W.C. Rontgen, Philos. Mag. 11, 308 (1881)
5. C.A. Bennett, Jr. and R.R. Patty, Appl. Opt. 21(1), 49-54 (1982)
6. J. Cao, J. Phys. D: Appl. Phys. 33, 200-206 (2000)
7. P. Charpentier, F. Lepoutre and L. Bertrand, J. Appl. Phys. 53, 608 (1982)
8. T. Hashimoto, J. Cao, and A. Takaku, Thermochim. Acta 120, 191-201 (1987)
9. T. Hashimoto and T. Tsuji, J. Therm. Anal. 40, 721-726 (1993)
10. H.J. Chang, J. Morikawa, T. Hashimoto, J. Appl. Polymer Sci. 99, 1104-1110 (2006)
11. A. Salazar, Europhys. J. 24, 351-358 (2003)
12. M.J. Adams, J.G. Highfield and G.F. Kirkbright, Anal. Chem. 52, 1260-1264, (1980)
13. A. Rosencwaig and J. Opsal, IEEE Trans. UFFC-33, No.5, (1986)
14. M.J. Adams, J.G. Highfield and G.F. Kirkbright, Anal. Chem. 49, No12 (1977)
15. A. Mandelis, J. Opt. Soc. Am. A 6, No. 2 (1989)
16. A. Mandelis and K. F. Leung, J. Opt. Soc. Am. A 8, no.1 (1991)
17. A. Mandelis and C. Wang, Anal. Sci. 17, (2001)
18. M.J. Adams and G.F. Kirkbright, Analyst 102, 281-292 (1977)
19. M.J. Adams and G.F. Kirkbright, Analyst 102, 678-682 (1977)
20. Z. Yugeng, S. Quinde and Z. Guiwen, Analyst 118, (1993)
21. H. Coufal, Polymer Engin. Sci. 31, No.2, (1991)
22. A. Phillip, P. Radhakrishnan, V.P.N. Nampoore and C.P.G. Vallabhan, J. Phys. D: Appl. Phys. 26, 836-838 (1993)
23. M.J. Adams, J.W. Einax. Anal. Bioanal. Chem. 382, 861-862 (2005)
24. K.U. Kwon, M.H. Choi, S.W. Kim, S.H. Hahn, D.J. Seong, J.C. Kim and S.H. Lee, Int. J. Thermophys. 21, No.2, (2000)
25. A. Bendada, Meas. Sci. Technol. 13, 1946-1951 (2002)
26. Photothermal Science and Techniques by D.P. Almond and P.M. Patel , Chapman and Hall (1996)
27. Principles of Applied Optics by P.P. Banerjee, Ting-Chung Poon, Aksen Associates (1991)
28. Infrared Detectors and Systems by E.L. Dereniak and G.D. Boreman, New York: Wiley (1996)
29. Engineering Thermodynamics, P.K. Nag , Tata Mcgraw-Hill, (1981)

30. Experiments in Heat Transfer and Thermodynamics by R.A. Granger, Cambridge University Press (1994)
31. Optical Methods of Engineering Analysis by G.L. Cloud, Cambridge University Press (1995)
32. Fundamentals of Engineering Thermodynamics by M.J. Moran, Pearson Prentice Hall (2004)
33. Thermal Sciences, an Introduction to Thermodynamics, Fluid Mechanics and Heat Transfer by M.C. Potter and E.P. Scott, Thomson- Brooks/Cole (2004)
34. CRC Handbook of Chemistry and Physics, ed. R.C. Weast et al, Boca Raton, CRC Press, edition 70 (1990-91)
35. L. Fabbri and F. Cernuschi, J. Appl. Phys. 82 (11) (1997)